

Spring 5-12-2018

CHARACTERIZATION OF WIDEBAND U-SLOT PATCH ANTENNAS THROUGH CHARACTERISTIC MODAL ANALYSIS AND COUPLED MODE THEORY

Tyler LaPointe

Electrical and Computer Engineering

Follow this and additional works at: https://digitalrepository.unm.edu/ece_etds



Part of the [Electrical and Computer Engineering Commons](#)

Recommended Citation

LaPointe, Tyler. "CHARACTERIZATION OF WIDEBAND U-SLOT PATCH ANTENNAS THROUGH CHARACTERISTIC MODAL ANALYSIS AND COUPLED MODE THEORY." (2018). https://digitalrepository.unm.edu/ece_etds/406

This Thesis is brought to you for free and open access by the Engineering ETDs at UNM Digital Repository. It has been accepted for inclusion in Electrical and Computer Engineering ETDs by an authorized administrator of UNM Digital Repository. For more information, please contact disc@unm.edu.

Tyler LaPointe

Candidate

Electrical and Computer Engineering

Department

This thesis is approved, and it is acceptable in quality and form for publication:

Approved by the Thesis Committee:

Dr. Christos Christodoulou , Chairperson

Dr. Mark Gilmore

John Borchardt

**CHARACTERIZATION OF WIDEBAND U-SLOT PATCH
ANTENNAS THROUGH CHARACTERISTIC MODAL
ANALYSIS
AND COUPLED MODE THEORY**

by

TYLER LAPOINTE

B.S. ELECTRICAL ENGINEERING

THESIS

Submitted in Partial Fulfillment of the
Requirements for the Degree of

**Masters of Science
Electrical Engineering**

The University of New Mexico
Albuquerque, New Mexico

May 2018

Acknowledgements

I am extremely fortunate to be surrounded by so many remarkable people to whom I owe the completion of this work. I would like to recognize these individuals as well as the organizations to whom my gratitude is due.

First, I would like to thank my advisor Dr. Christos Christodoulou as well as my committee members Dr. Mark Gilmore, Dr. Lucas Feldner, and John Borchardt for their mentorship, guidance, and input throughout this journey.

I would also like to thank Dr. Matthew Young for his expertise, knowledge, and suggestions as this paper was coming together. Additionally, I would like to recognize Alex Bates and Christopher Gibson for their support and encouragement.

I am indebted to the Circuit Shop for donating their time and the fabricated antenna boards that were tested through this research. I'm also grateful for the tools and facilities provided by Sandia National Laboratories and the University of New Mexico.

Finally, I am endlessly thankful for the sacrifices made by Erin and Tallen whose unbounded love, belief, and support mean the world and are the sources of my strength, achievements, and success.

**CHARACTERIZATION OF WIDEBAND U-SLOT PATCH ANTENNAS
THROUGH CHARACTERISTIC MODAL ANALYSIS
AND COUPLE MODE THEORY**

by

Tyler LaPointe

B.S., Electrical Engineering, University of New Mexico, 2016

M.S., Electrical Engineering, University of New Mexico, 2018

ABSTRACT

Microstrip patch antennas (MPAs) are utilized in many applications as they are easy to produce and are thin, versatile, light weight, cheap, and reliable. One of the drawbacks of MPAs, however, is their narrow bandwidth, typically three to ten percent. Fortunately, a perturbation exists capable of resolving this issue known as the U-slot which can increase the operational bandwidth of a single layer MPA to around 30 percent. Often it is reported that the wideband performance of this structure results from the existence of two resonators, the patch and the U-shaped slot. While this is true, the very nature of this dual resonance and its relationship to wide bandwidth has not been well defined as misconceptions about the design are common. A few of the more significant publications on U-slot MPAs have recently utilized characteristic modal analysis

(CMA) as a figure of merit to judge and/or improve existing U-slot design methods. However, it is demonstrated that by combining CMA with Coupled Mode Theory (CMT), it is possible to explain the U-slot MPA's wideband behavior and operational characteristics. A complete analysis of which is presented through a culmination of U-slot MPA simulations, circuit models, CMT analysis, and fabricated U-slot MPA designs. Lastly, an improved approach to wideband U-slot MPA design is demonstrated based on the discovered fundamental operational characteristics.

TABLE OF CONTENTS

CHAPTER 1 BACKGROUND.....	1
The Microstrip Patch Antenna.....	1
Characteristic Modal Analysis.....	7
U-Slot Patch Antennas.....	9
CHAPTER 2 THEORY & ANALYSIS.....	13
Simulation and Fabrication of the Original U-Slot MPA.....	13
Identifying Resonant Modes With CMA.....	23
The U-Slot MPA Circuit Model.....	29
Coupled Mode Theory.....	33
CHAPTER 3 EXPERIMENTAION & U-SLOT DESIGN METHDOLOGY.....	44
Designing a 2.5 GHz U-Slot MPA.....	44
Conclusions.....	69
Future Work.....	71
REFERENCES.....	73

Chapter 1

Background

The Microstrip Patch Antenna

The MPA consists of a metallic radiating planar surface mounted upon a dielectric substrate backed by a ground plane (Figure 1). The microstrip topology was introduced in the 1950's by Grieg and Englemann [1] for the application of microwaves and first utilized for antennas by Deschamps in 1953 [2]. However, the MPA did not become popular until the developments of printed circuit board (PCB) technology and consistent dielectric manufacturing which made the MPA more efficient, easy to produce, thin, lightweight, cheap, reliable, and compatible with other planar circuit topologies.

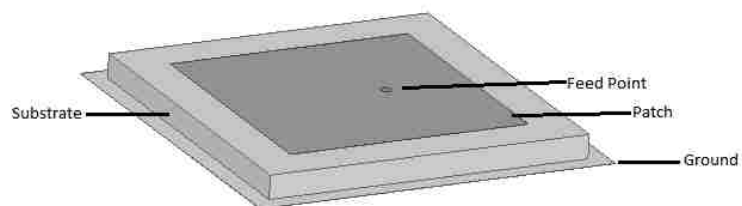


Figure 1. MPA Configuration

MPAs can be made in many different shapes and sizes and are utilized for operational frequencies between 0.3 - 40 GHz, with size and efficiency limiting their use elsewhere. MPAs can be fed by microstrip transmission lines, apertures, edge coupling, or coaxial cables and may be linear, polar, or elliptically polarized. The feed type, polarization, shape, and size of an MPA is

heavily dependent on the intended application and the operational frequency. Applications consist of satellite communication, cell phones, wireless internet, direct broadcast television, and telemetry data systems. The main shortcomings of a typical MPA consists of low radiation efficiency, narrow bandwidth (3%-10%), and unsuitability for use at higher power levels.

When excited, MPAs radiate due to fringing fields on the patch's edges caused by strong surface currents and the electric field between the patch and the ground plane (Figure 2).

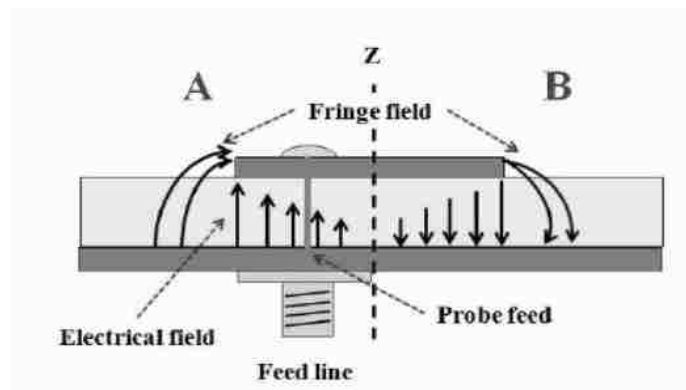


Figure 2. Electric Field Lines of an MPA [3].

Although MPAs are simple in structure, they have proved difficult to analyze. The first method developed to analyze the MPA was introduced by Munson [4] and is known as the transmission line model which represented an MPA by a section of transmission line having lossy loads at each end which characterize the patch's radiating edges (Figure 3).

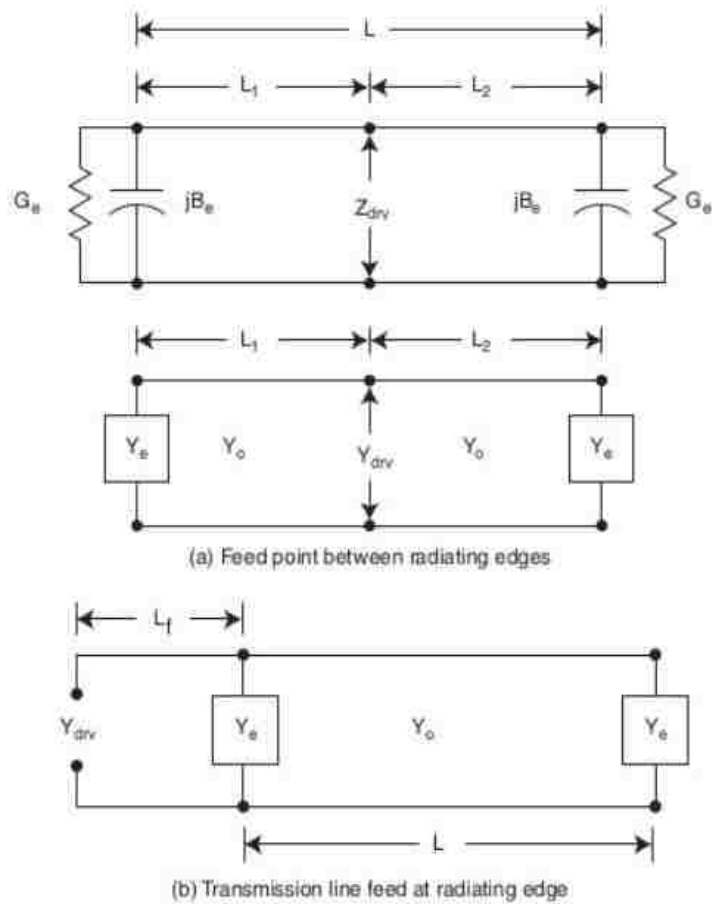


Figure 3. Transmission Line Model of a Rectangular MPA [5].

By choosing any point along the length of the transmission line, the input impedance of a given feed point can be calculated and is often expressed in terms of admittance. This initial transmission line model is limited by the fact that it can only be used when one mode is resonant, it is inaccurate for thin substrates, applies only to rectangular shapes, and it assumes currents flow along the transmission line in only one direction.

The second MPA analysis method is known as the cavity model, developed by Lo et al [6] which further describes the MPA as a lossy resonant cavity with open circuit, perfect magnetic conductor (PMC) conditions on the cavity's vertical edges and short circuit, perfect electric conductor (PEC) conditions on the cavity's horizontal edges (Figure 4).

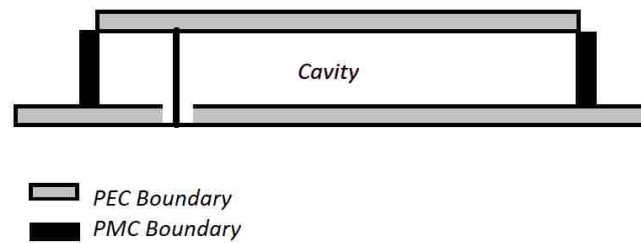


Figure 4. Cavity Model of an MPA

In Figure 4, the PEC boundaries represent the patch and the ground plane while the PMC boundaries support a voltage distribution at the MPA's edges. Due to this configuration, only certain modes can exist inside the cavity. Using the cavity model, it is possible to describe these MPA operational modes according to the MPA's geometry. For example, a rectangular MPA will operate in what is referred to as the transverse magnetic (TM) mode. The mode designation TM_{mn} describes the condition where the magnetic field in a system is transverse to the direction of wave propagation with the subscript m designating the number of half wave electric field variations along the MPA's x dimension and the n subscript designating the number of half wave electric field variations along the MPA's y dimension. The TM_{01} and TM_{10} mode configurations and their electric field

distributions are shown in Figure 5 and 6 below. These two mode configurations are the most commonly used modes for MPA operation.

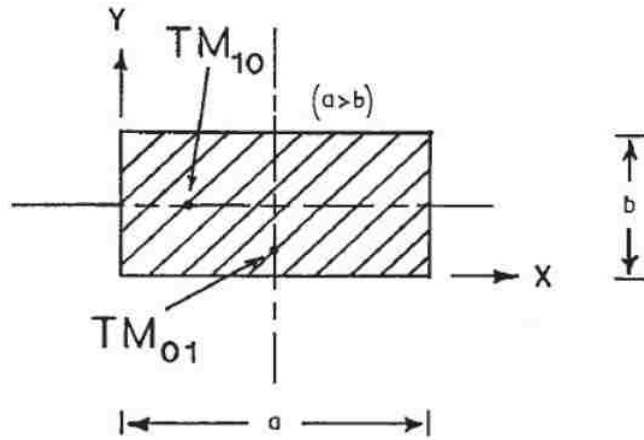


Figure 5. TM_{10} & TM_{01} Mode Configurations [5].

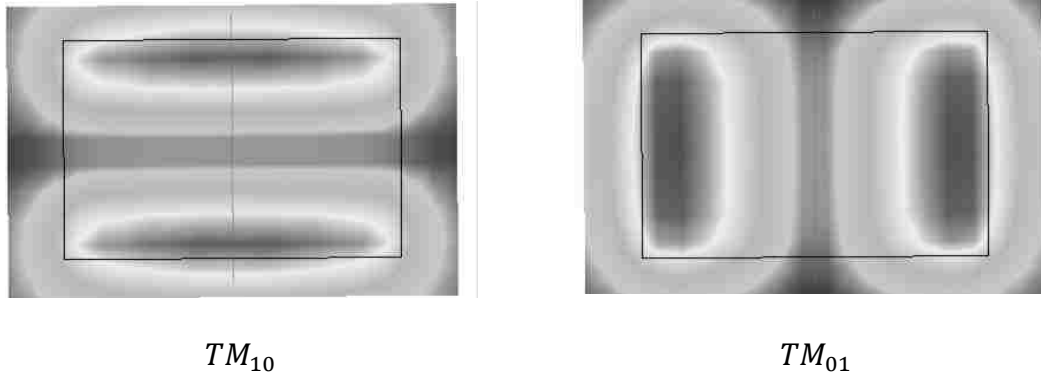


Figure 6. Electric Field Distributions

Initially, the cavity model was limited to thin substrates and did not account for feed probe inductance while having similar current approximations used in the transmission line model. Over the years the cavity model has been refined and improved to include probe feed inductance and higher order modes [7], [8].

However, the model is still limited to substrate thickness that are much less than the wavelength of the operational frequency and is unable to analyze multilayered or complex MPA designs.

It was not until the 1980's, when the advancement of computers led to the use and development of computational electromagnetic (CEM) analysis, that MPA modeling achieved an elevated level of fidelity. One such CEM analysis method, known as the method of moments (MoM), is credited for becoming the first analysis method able to completely characterize the MPA by eliminating current distribution approximations that limited the cavity and transmission line models. In the case of antenna analysis, MoM can be used to solve an integral equation of the general form representative of a given radiation problem in terms of the unknown currents. Such an equation, representative of a dipole antenna, is seen in equation 1.

$$-\int I(z')K(z, z')dz' = E'(z) \quad (1)$$

Where I represents the unknown currents, K stands for the kernel function dependent upon the equation formulation, and E is the electric field. More importantly for this paper's purpose, the MoM may also be expressed in a linear algebraic form by requiring the total tangential electric fields on a given conducting body to be equal to zero as expressed in equation 2 where $E_{tan,s}$ represents the scattered electric field from a surface current and $E_{tan,i}$ represents

the tangential component of the incident electric field from an internal or external source.

$$0 = E_{tan,s} + E_{tan,i} \quad (2)$$

If the surface currents related to the fields in equation 2 are approximated by Rao-Wilton-Glisson subdomain functions, the above expression can be re-written into the impedance matrix form seen in equation 3. The steps involved in this process are covered in [9].

$$[Z_{mn}][I_n] = [V_m] \quad (3)$$

This representation of the MoM provides the basis upon which a closely related CEM method, known as characteristic modal analysis (CMA), is founded.

Characteristic Modal Analysis

CMA was pioneered in the 60's by Garbacz [10] however its capability was limited until the theory was simplified for computing currents and their related fields by Harrington and Mautz in 1971 [11], [12]. CMA is popular due to its ability to separate the electromagnetic analysis of a given conducting body into its individual current modes whereas other CEM methods analyze the sum or superposition of all supported modes. The individual current modes are only dependent on the shape and size of the conducting body providing unique insight into the physical characteristics of a given antenna. Ultimately these

characteristic modes define a surface's near and far-fields which describe the radiating properties of the structure. Characteristic modes are obtained by solving a weighted eigenvalue equation that is derived from the MoM impedance matrix, equation 3, which results in the matrix eigenvalue equation, equation 4, for a given conducting body,

$$[X]J_n = \lambda_n[R]J_n \quad (4)$$

Where J_n represents the surface supported eigen currents, λ_n represent the eigenvalues, and the MoM impedance matrix $[Z]$ is represented in terms of its real and imaginary components, $[X]$ and $[R]$. In this form, the eigenvalues, λ_n , are the focus as they represent the complex power balance or difference between the stored magnetic and electric energy in a mode over a frequency range of interest as expressed in equation 5

$$\omega(W_m - W_e) = \lambda \quad (5)$$

When the energy difference becomes equal to zero, the mode will become resonant. Modes whose eigenvalues start negative are referred to as capacitive and have a chance of becoming resonant. Modes whose eigenvalues start positive are referred to as inductive and will not become resonant. An in-depth explanation of CMA's application to antenna design was conducted by Cabedo in 2007 [13]. Increased computational power has made it possible to compute the

characteristic eigenvalues and currents of a given body over a wide range of frequencies. Feko, a MoM code by Altair, is one such CMA analysis tool which will be utilized for the CMA simulations in this paper.

U-Slot Patch Antennas

First published by Huynh and Lee in 1995 [14], the addition of the U-shaped slot was shown to improve an MPA's bandwidth to over 40 percent. Huynh and Lee's original U-slot MPA design had an air substrate that was 1.06 inches thick with an operational frequency of 900 MHz and was center fed with a coaxial probe. Huynh and Lee's U-slot diagram and their test results are shown in Figures 7-9.

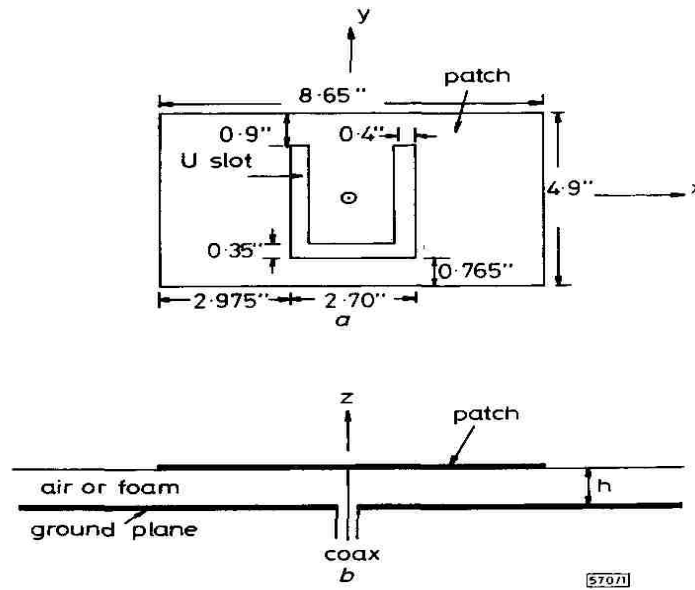


Figure 7. Geometry of U-Slot MPA a) Top View, b) Side View [14]

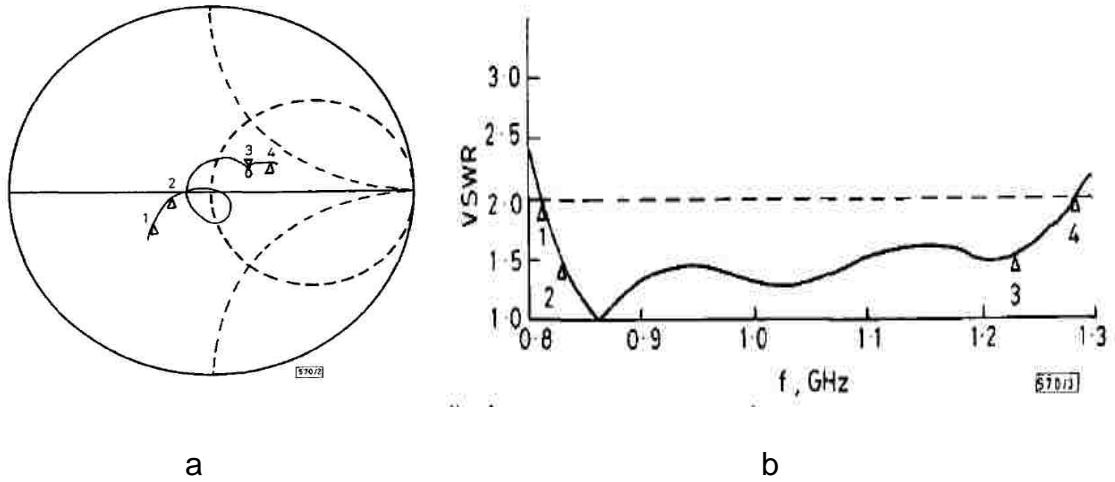


Figure 8. a) S_{11} Impedance Locus Plot, b) VSWR Plot [14]

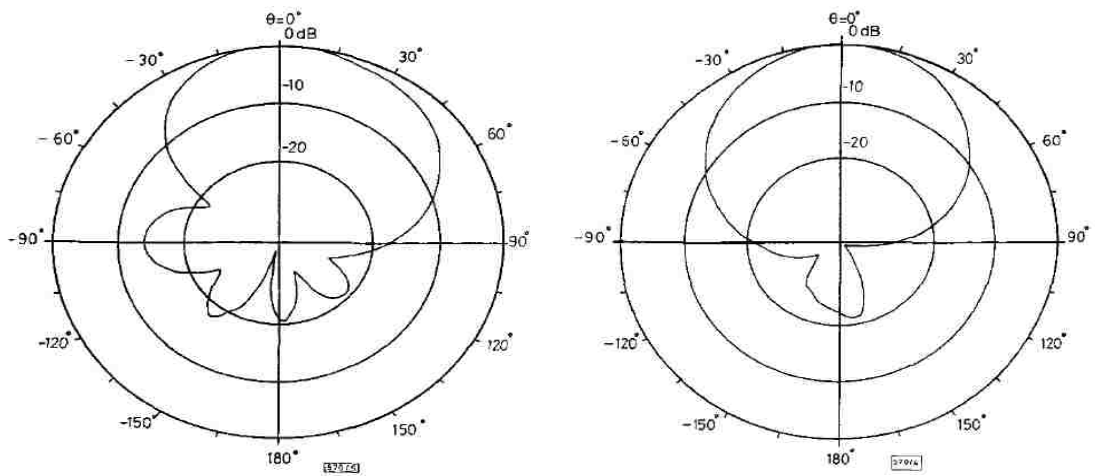


Figure 9. U-Slot Far-Field Patterns [14]

It is worth noting that the looped impedance locus seen in Figure 8a is characteristic of coupled systems and is observed in the response of coupled filters and waveguides.

At the time of Huynh and Lee's publication, it was reported that although the feed probe was relatively long, it did not contribute any inductive reactance to the overall input impedance of the MPA as it was effectively canceled out by the capacitive reactance introduced by the existence of the U-shaped slot. Although this MPA perturbation solved the narrow bandwidth characteristics, it was not well understood. It was hypothesized that the increased bandwidth was due to the existence of two radiators, the patch and the U-slot, which remains the extent of the explanation as to the author's knowledge no quantitative explanation, theory of operation, or systematic design method of the U-slot MPA exists. Over the years the achievable bandwidth of U-slot MPAs has been shown to be closer to 30% [15] [16] [17] [18]. Nevertheless, it is a significant improvement for a single layer MPA.

Since the Huynh and Lee original publication, U-slot MPA's have been adapted into a wide variety of application and uses. Although not wideband, the U-slot MPA can be used as a multi band MPA capable of radiating at several separate frequencies. These MPA's often include multiple U-slots in a single patch whose existence creates notches within the bandwidth (Figure 10) [19].

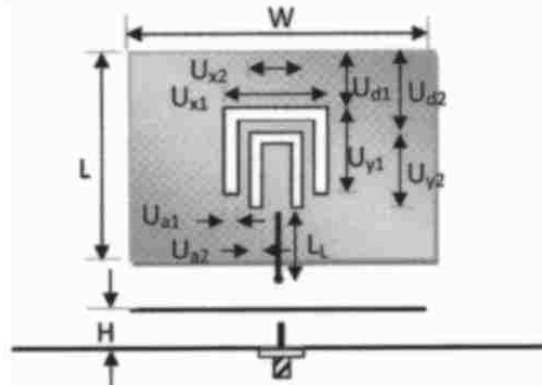


Figure 10. Multiband U-Slot MPA [19]

In addition, it has also been shown by Tong and Wong [20] that the U-slot MPA can be circularly polarized when the slot lengths are uneven as seen in Figure 11.

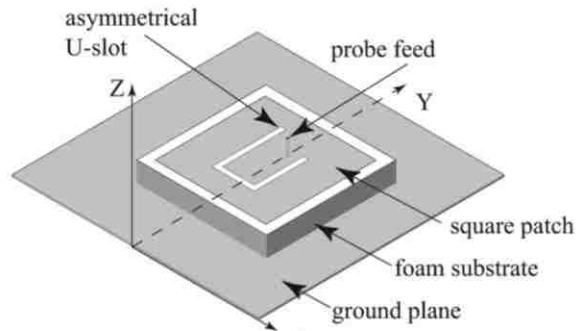


Figure 11. Circularly Polarized U-Slot MPA [20]

Multiple, single U-slot MPA's can be combined to form antenna arrays as demonstrated by Wang, Huang, and Fang [21] where the array shown in Figure 12 has a bandwidth of 18% at a center frequency of 6.22 GHz.

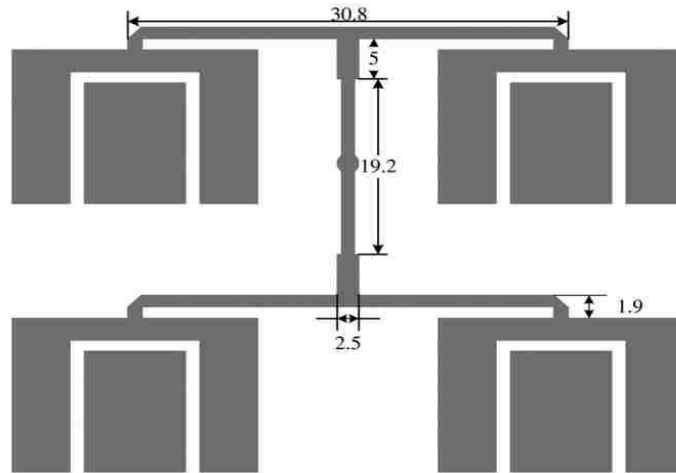


Figure 12. U-Slot MPA Array [21]

More recently, CMA has been used to rate various empirical U-slot MPA design techniques as well as determine the effects of substrate thickness, U-slot dimensions, feed locations, and feed probe dimension on radiation characteristics [15], [22]. CMA has also been used to improve the axial ratio and the cross-polarization performance of circular polarized U-slot MPA designs [23].

Chapter 2

Theory & Analysis

Simulation & Fabrication of the Original U-Slot MPA

To analyze and observe the behavior of the U-slot antenna, a driven simulation of the original U-slot MPA was created in Feko, seen in Figure 13 below. The intent is not to achieve the exact results reported in the publication nor are they expected as information about how the original U-slot MPA was

fabricated and tested is incomplete. However, comparable results should be achieved to provide an operational wideband U-slot MPA for study. The driven simulation is modeled with all the original dimensions, an air substrate, and a rectangular probe having four times the width of the reported original probe feed diameter.

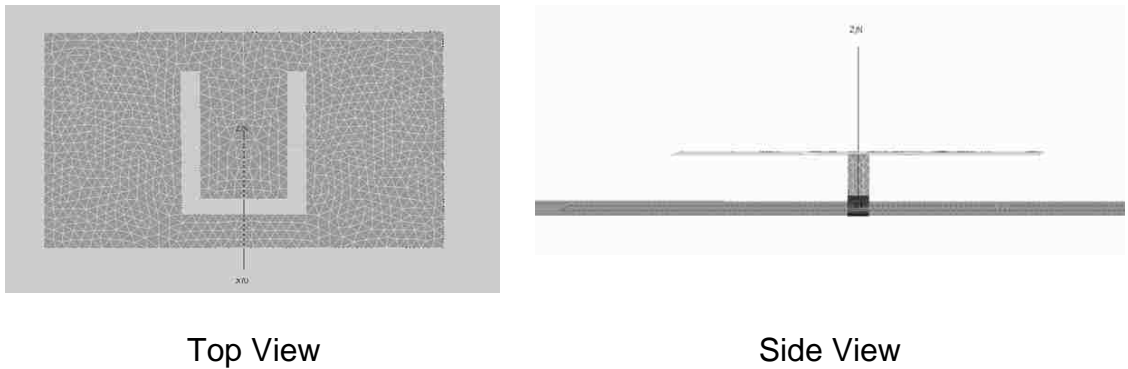


Figure 13. Model of Original U-Slot MPA

The driven simulation results are shown in Figure 14 and 15 below.

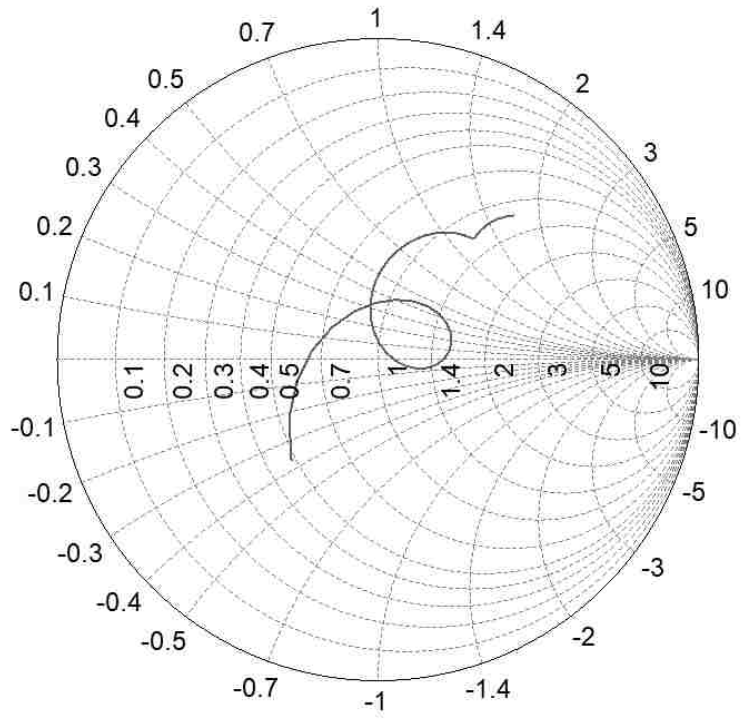


Figure 14. Simulated S_{11} Impedance Locus

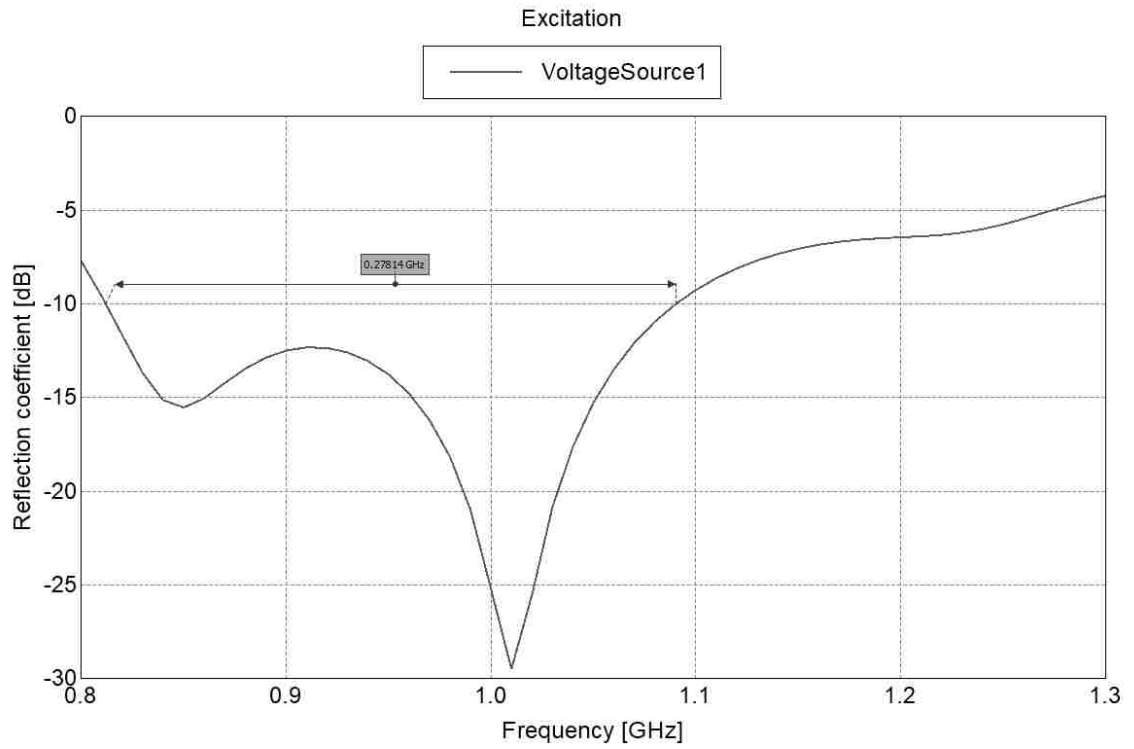
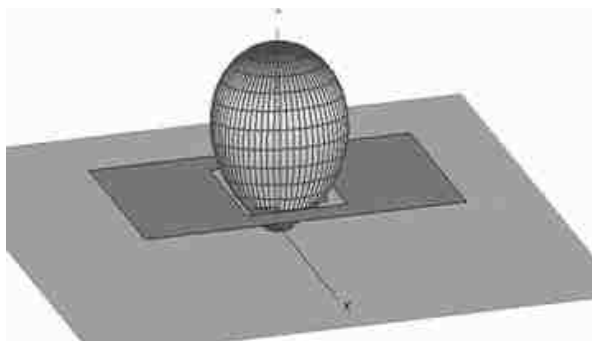
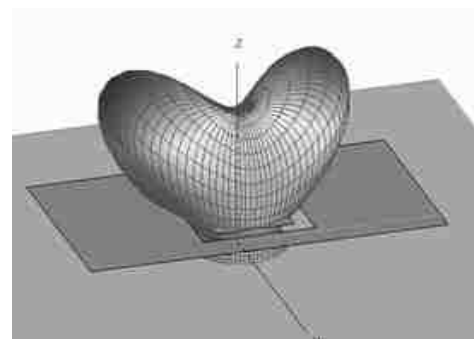


Figure 15. Simulated S_{11} Log Magnitude

One of the discrepancies noticed between the results in the original U-slot publication and the results in Figure 14 was that the long feed probe appeared to add appreciable inductance to the patch's input impedance demonstrated by the upwards shift in the impedance locus on the Smith chart. As the radiation pattern was observed over the reported bandwidth, it became unstable at higher frequencies and morphed from the desirable broadside patch pattern to the less desirable pattern depicted in Figure 16b.



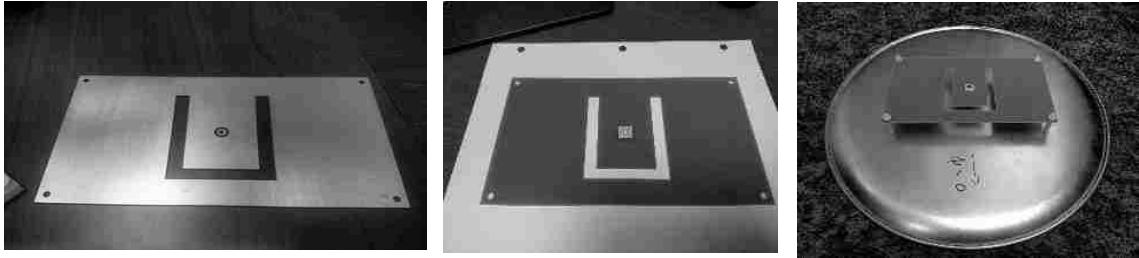
a) 0.8-1.17 GHz



b) 1.17-1.3 GHz

Figure 16. Far-Field Radiation Pattern

If the U-slot MPA's bandwidth could be increased beyond 30%, it would not likely be useful at the upper end of the frequency band due to this change in radiation pattern. With the above simulation observations, a physical U-slot antenna was fabricated for further analysis (Figure 17).



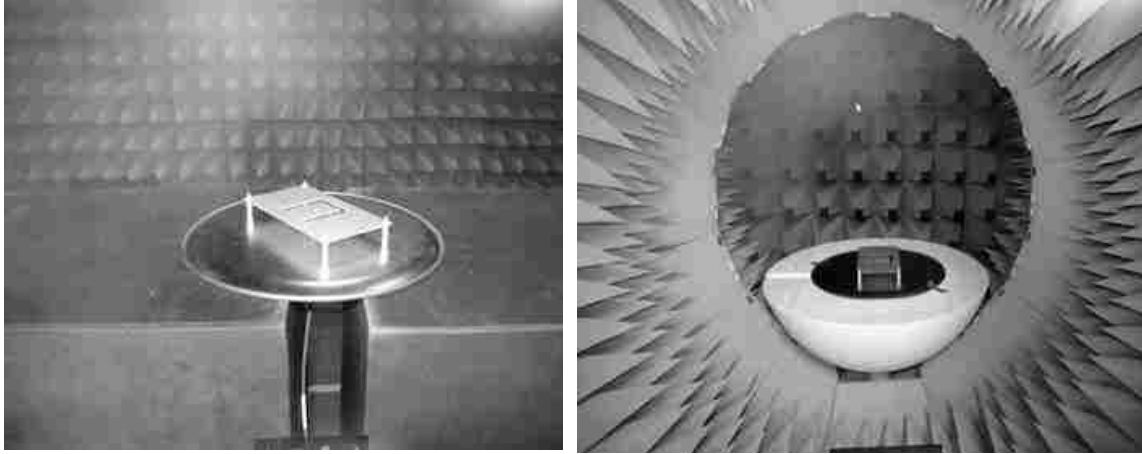
a

b

c

*Figure 17. a) Fabricated U-Slot MPA side 1, b) Fabricated U-Slot MPA side 2
c) Complete Test Assembly*

For test purposes the Huynh and Lee U-slot MPA replica was created on 62 mil FR4 and inverted such that only air was in between the patch metallization and the 16" diameter circular ground plane. Simulations representing the complete test assembly showed this orientation had the least effect when compared to the performance of the design without the FR4. It was also discovered that any dielectric material other than air inside the U-shaped slot adversely affected the antenna's performance, requiring the U-shaped slot be cut into the FR4 as well. Lastly, a series tuning capacitor was included to compensate for probe feed inductance [24] (note small metal square at the center of Figure 17b). The fabricated replica was then tested with a FieldFox vector network analyzer (VNA) in an anechoic chamber as well as a Satimo Starlab 18 near-field antenna chamber. Both test setups are shown in Figure 18.



a

b

Figure 18. a) VNA Test in Anechoic Chamber, b) Satimo Chamber Test

The VNA and Satimo test results are shown in Figures 19-23.

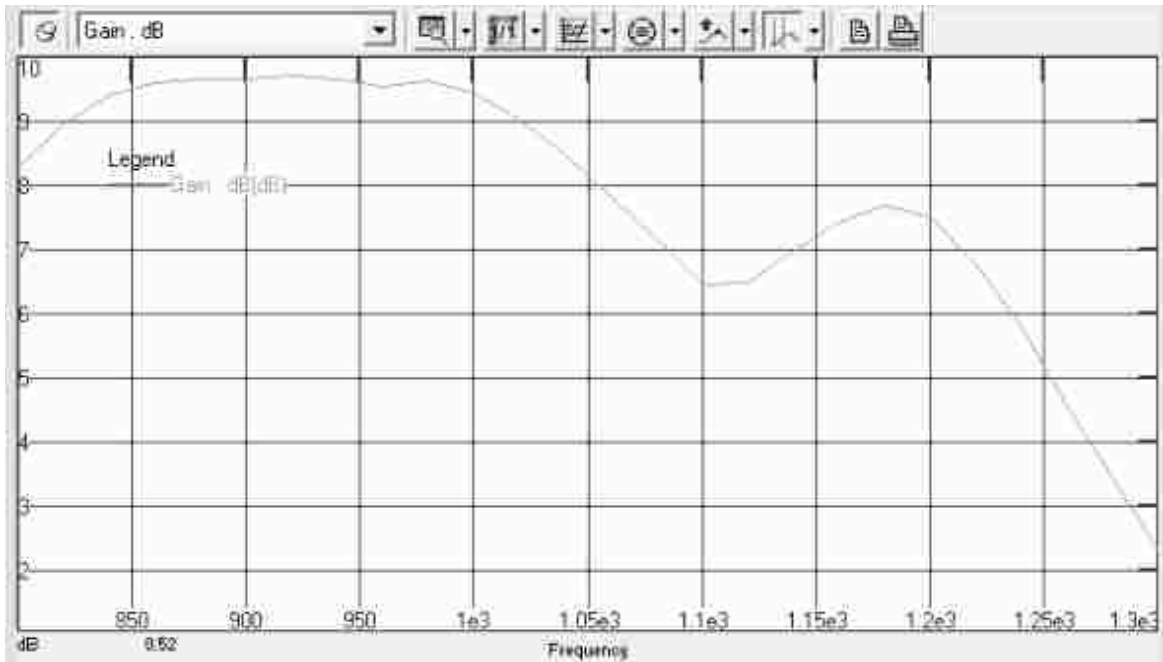


Figure 19. Measured Satimo Gain Results



Figure 20. Measured Satimo Efficiency Results

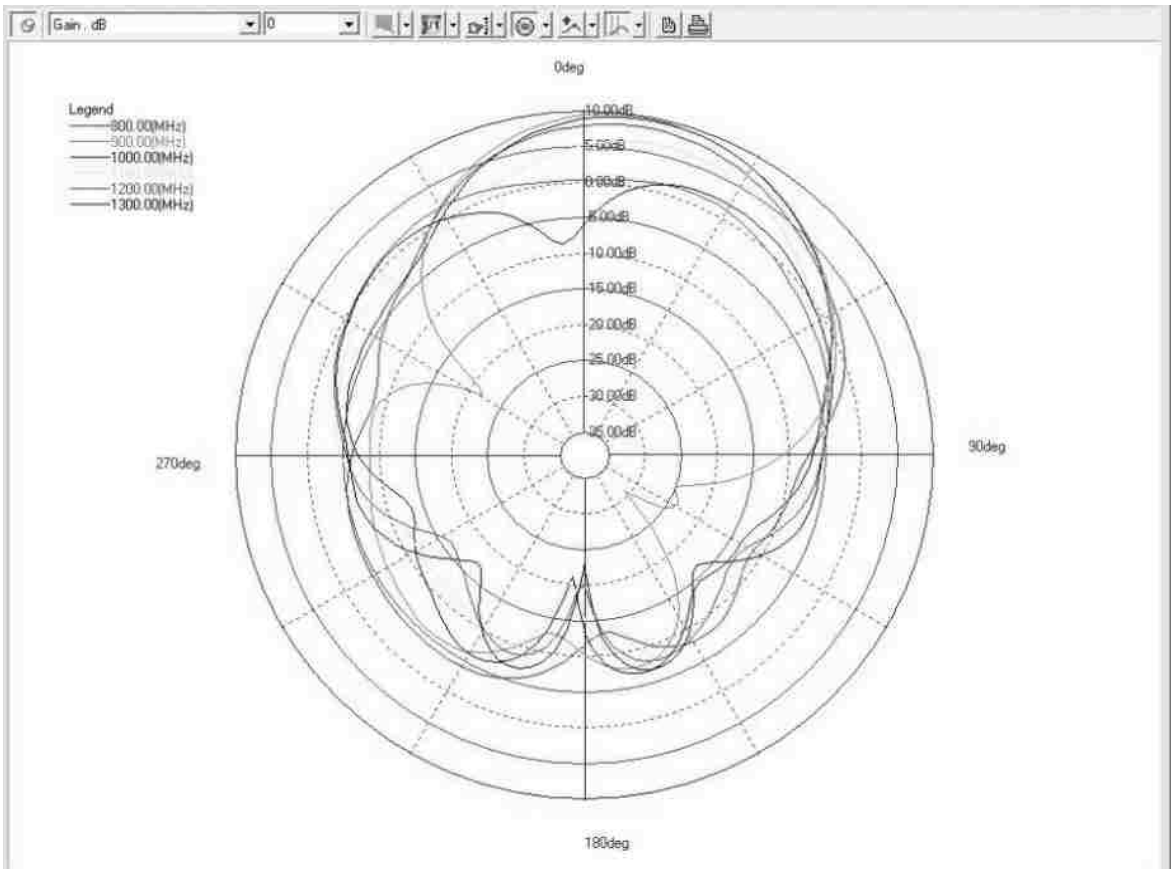


Figure 21. Measured Satimo Far-Field Pattern View 1

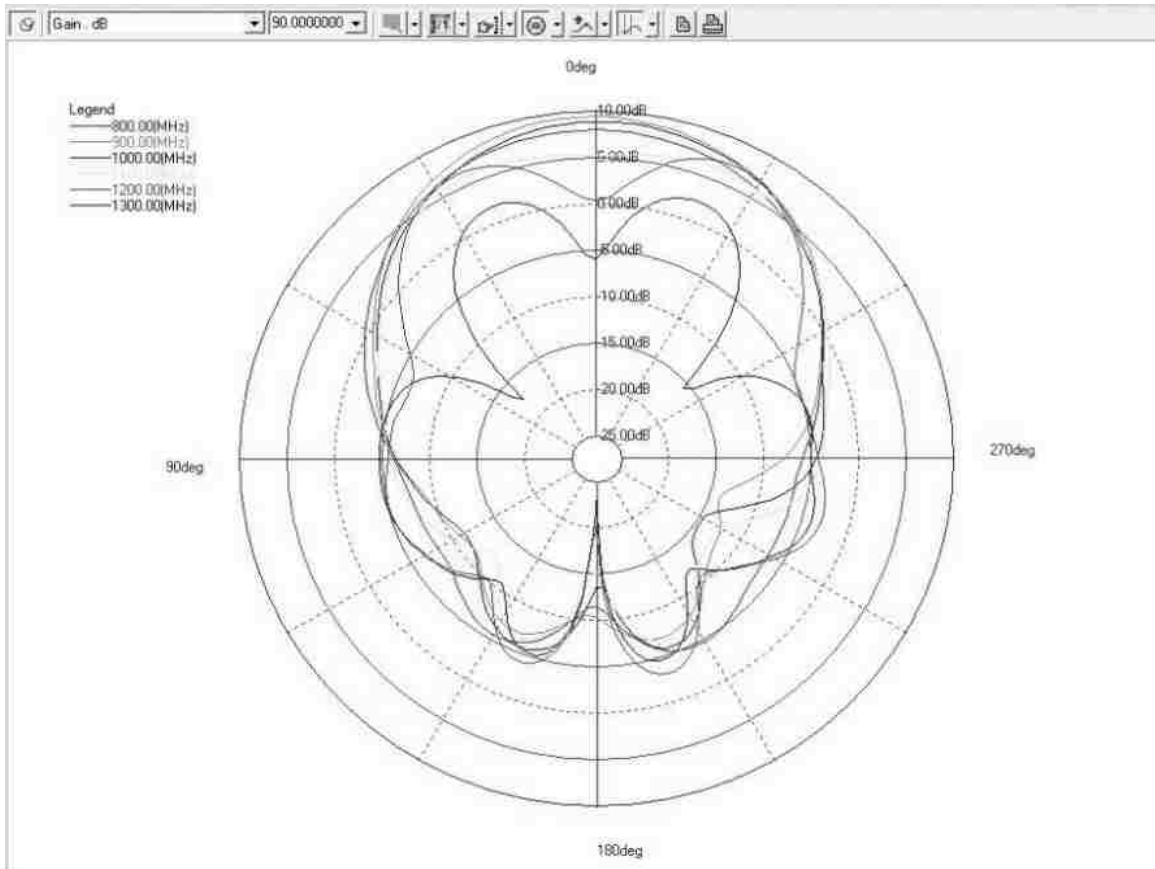


Figure 22. Measured Satimo Far-Field Pattern View 2

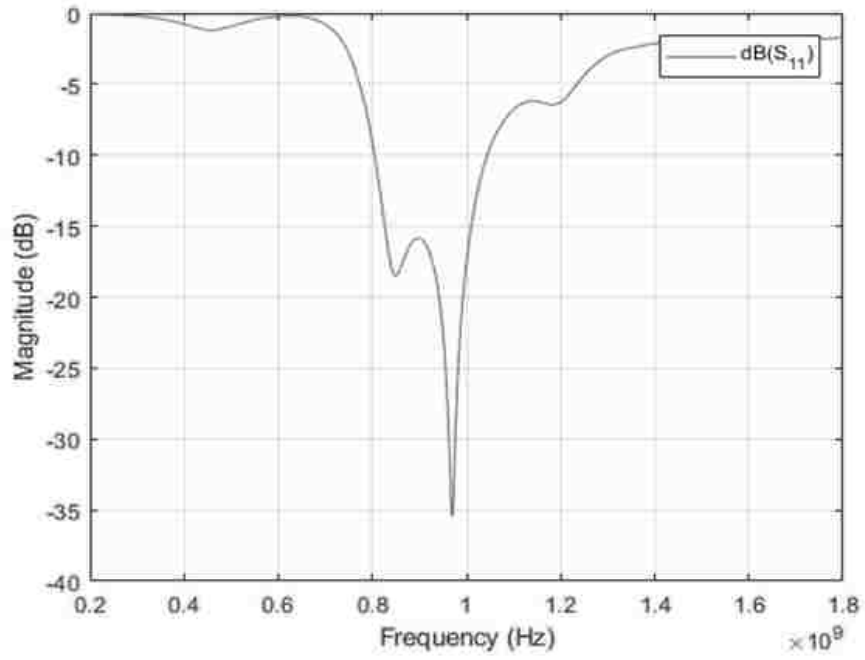


Figure 23. VNA Measured S_{11} Log Magnitude

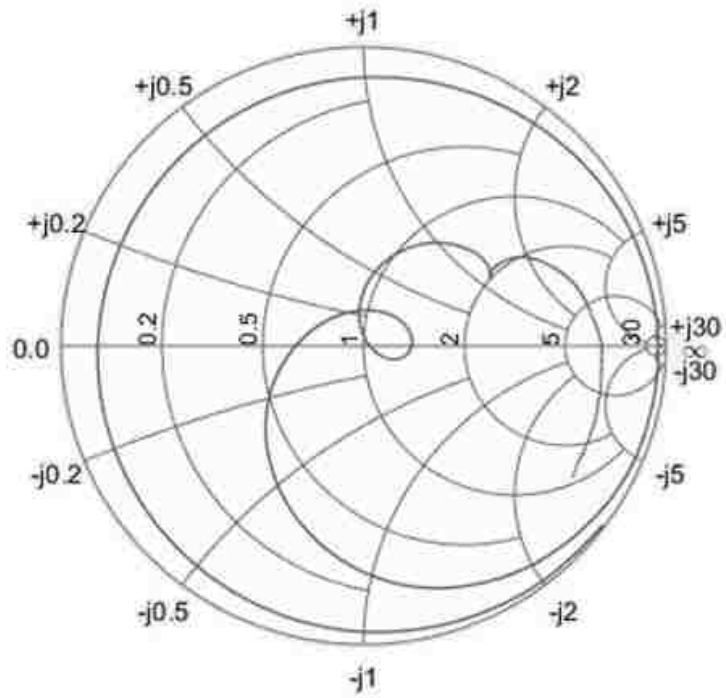


Figure 24. VNA Measured S_{11} Impedance Locus

The impedance locus plot of Figure 24 demonstrates the tuning capacitor on the fabricated U-slot MPA could be smaller to fully center the loop in the Smith chart. Without the tuning capacitor the loop would have been much further off to the upper right of the Smith chart. The far field test results in Figure 21 and 22 shows the radiated pattern becomes unstable at the upper end of the frequency bandwidth. The test results in Figure 23 confirms the 30% bandwidth was achieved.

Identifying Resonant Modes With CMA

With the driven simulation and the test results of the fabricated U-slot MPA, the next analysis step was to conduct a CMA simulation to observe the U-slot MPA's modal behaviors. The eigenvalue plots for the first four resonant modes are shown in Figure 25.

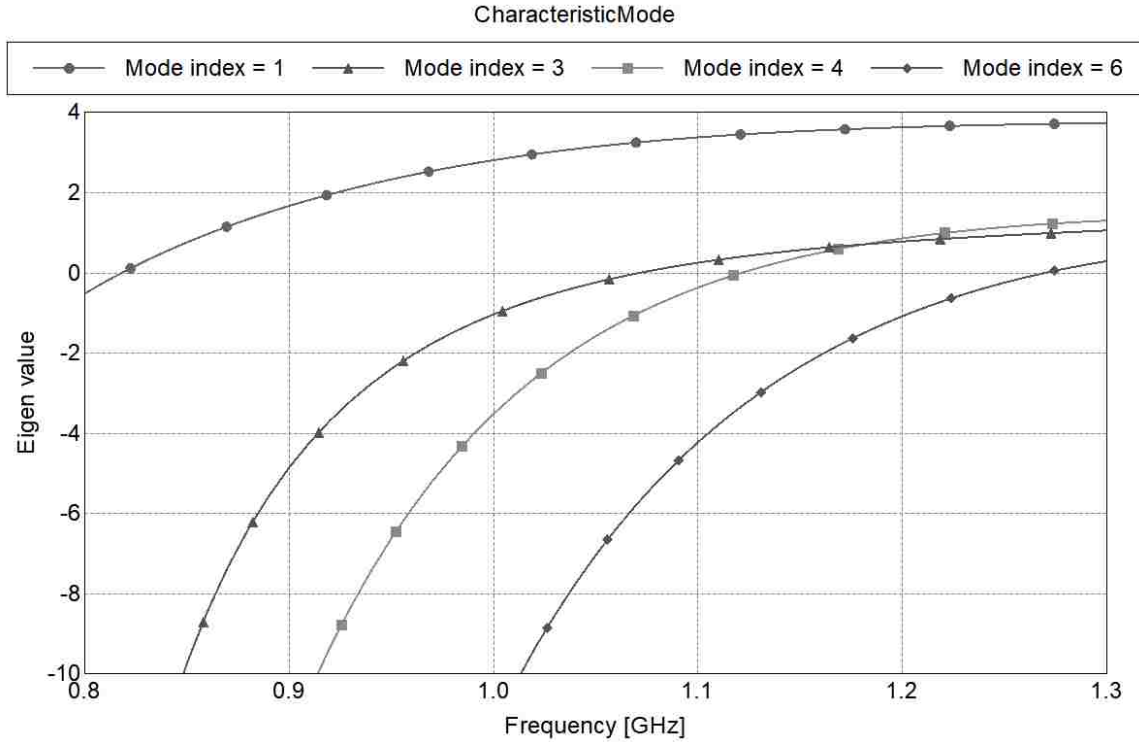
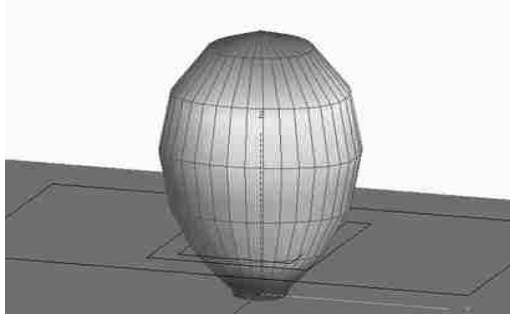
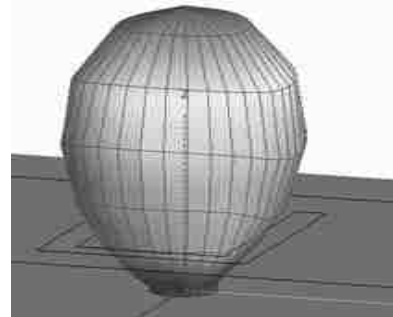


Figure 25. U-Slot MPA Eigenvalues of First Four Resonant Modes

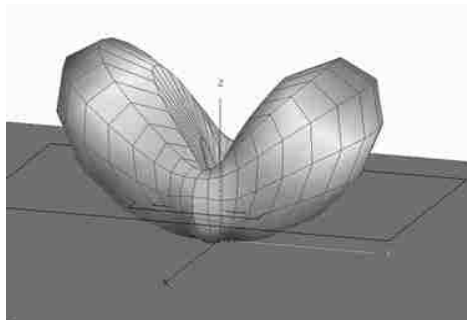
From Figure 25 it is observed that the first four resonant modes resonate at 0.81 GHz, 1.12 GHz, 1.2 GHz, and 1.28 GHz. Additional information can be gained by viewing the far-field radiation patterns of the resonant modes at their resonant frequencies, seen in Figure 26.



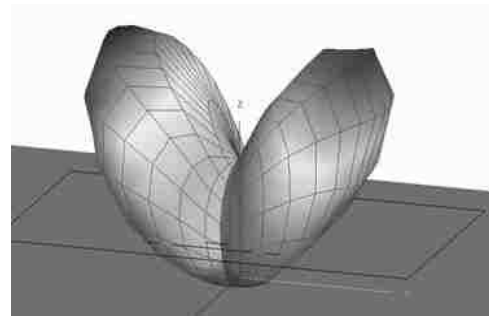
Mode 1



Mode 3



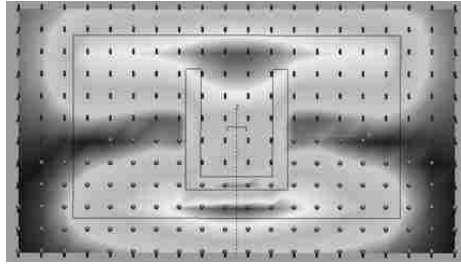
Mode 4



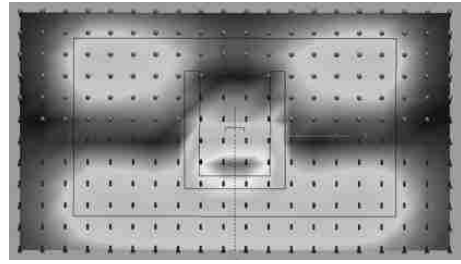
Mode 6

Figure 26. CMA Far-Fields

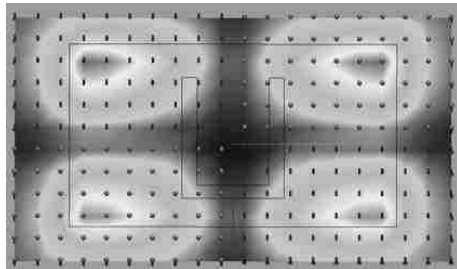
From Figure 26 it is noted that modes 1 and 3 have desirable MPA radiation patterns while modes 4 and 6 have less desirable radiation patterns like the patterns previously noted at higher frequencies. It is also important to observe the near-field patterns of the first four resonant modes (Figure 27).



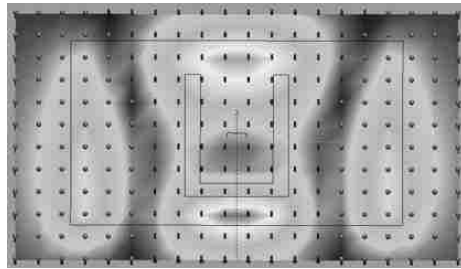
Mode 1



Mode 3



Mode 4



Mode 6

Figure 27. CMA Near-Fields

The near-field plots show modes 1 and 3 have a “perturbed TM_{10} mode” excitable with a center feed while the pattern of mode 4 shows it cannot be excited as there is a vertical electric field null directly across the center of the pattern. Therefore, any of the undesired radiation pattern at higher frequencies must be due to the contribution of mode 6 becoming resonant at higher frequencies. Additionally, the input impedance of each mode is shown below in Figure 28.

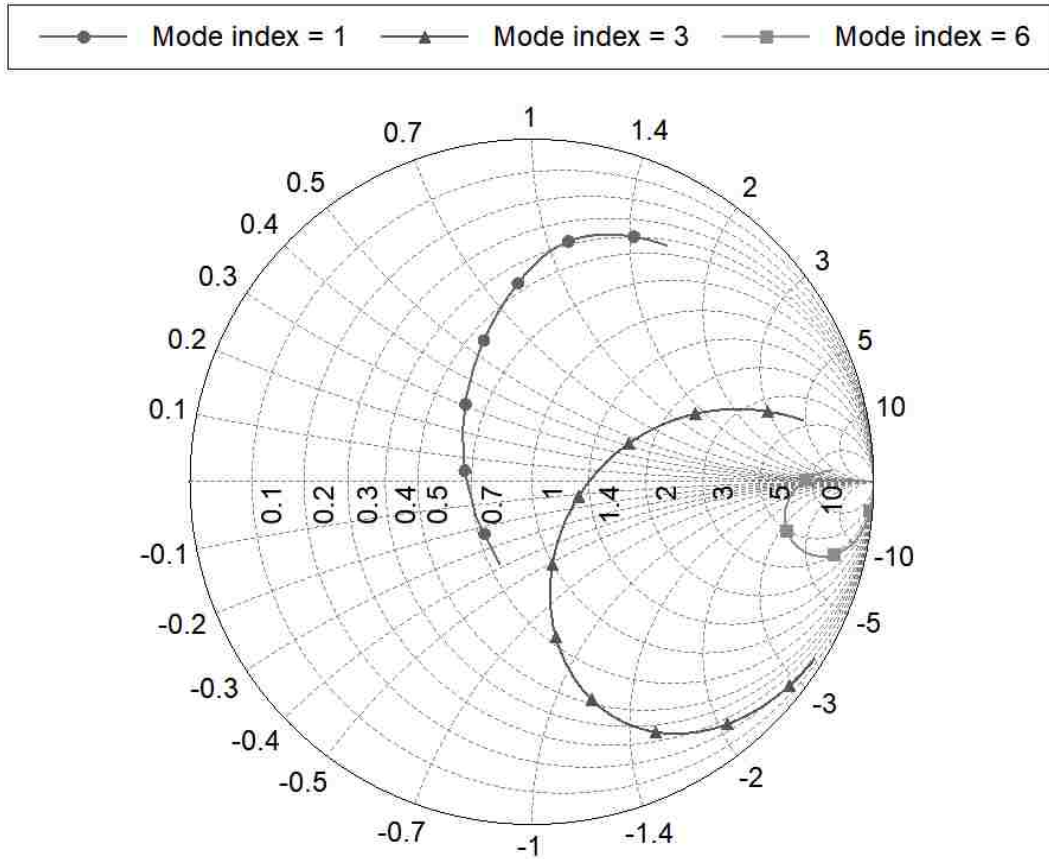


Figure 28. Impedance Locus of the First Four Resonant Modes

From the input impedance plots it was observed that mode 4's input impedance was infinite as predicted from its near field pattern, while mode 6 appears to be sub-resonant. If a loop is to be formed in the Smith chart, it must be due to the combined impedances of modes 1 and 3. Lastly, the power distributions for modes 1, 3, and 6 are shown in Figure 29.

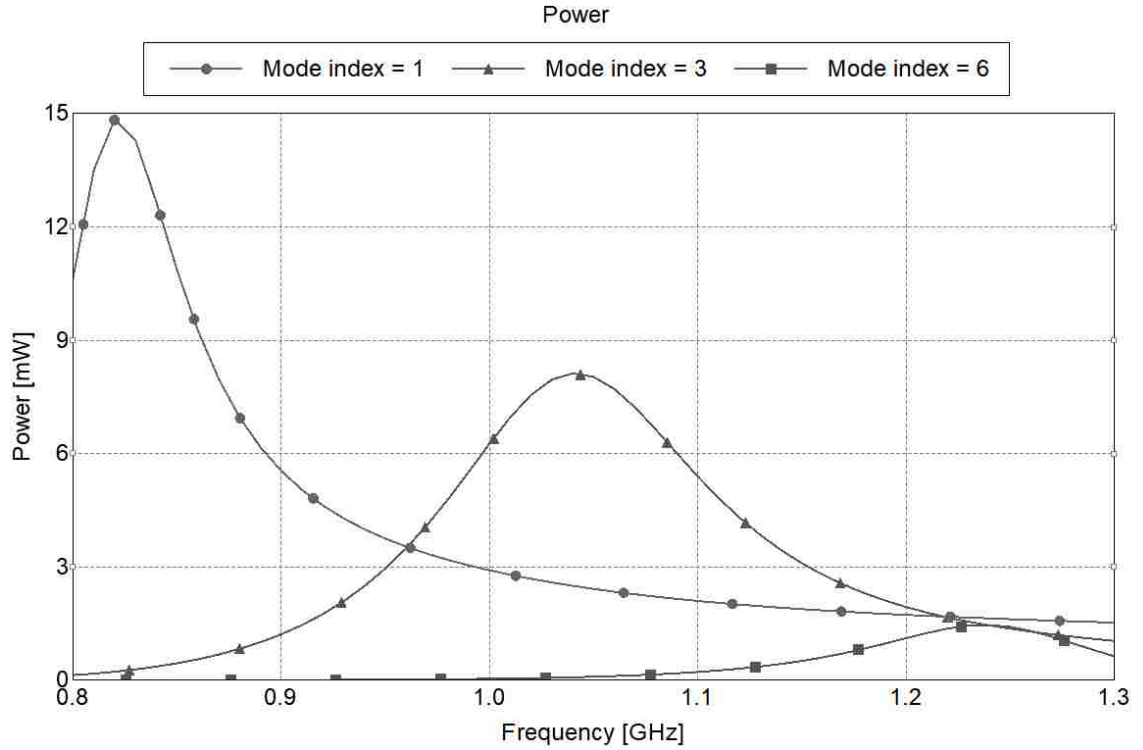


Figure 29. Power Distribution of Resonant Modes

From Figure 29 it is shown that most of the power over the operational bandwidth is contained within modes 1 and 3. From the power distribution plot it is possible to calculate the Q of each mode with equation 5.

$$Q = \frac{f_c}{BW_{3dB}} \quad (5)$$

Equation 5 results in a Q of about 7 for each mode respectively, a value expected for wideband operation. By analyzing all the modal information provided by CMA,

it is possible to arrive at the conclusion that modes 1 and 3 are the main radiating mechanisms in the U slot antenna due to the following three reasons:

- 1) Modes 1 and 3 have radiation patterns observed over the 30% bandwidth
- 2) Modes 1 and 3 are excitable with a center feed probe
- 3) Most of the power over the 30% bandwidth is in these two modes

With the two U-slot operational modes identified, understanding how their combined impedances form a loop in the Smith chart is possible by creating a circuit model of the U-slot MPA.

The U-Slot MPA Circuit Model

To examine and understand how the combination of modal impedances form a loop in the Smith chart, it is helpful to develop a circuit model of the U-slot MPA. Each resonant mode's individual input impedance can be represented by a series *LRC* circuit such that when combined in parallel the total impedance of the circuit will reflect the total input impedance of the U-slot MPA. The relationship between characteristic modes and their representative circuit models is explained by Adams and Bernhard [25]. Using Agilent's ADS circuit simulation software, it is possible to create a U-slot circuit model from two series *LRC* circuits which represent modes 1 and 3. If done correctly, the circuit will have an impedance locus matching that of the simulated and physical U-slot antenna. This can be

achieved by setting the L and C values as a function of each mode's characteristic impedance (Z_c) at their respective resonant frequencies (f_r). The R and Z_c values can be tuned to match the overall impedance of the U-slot MPA. The resulting representative U-slot circuit model is shown in Figure 30.

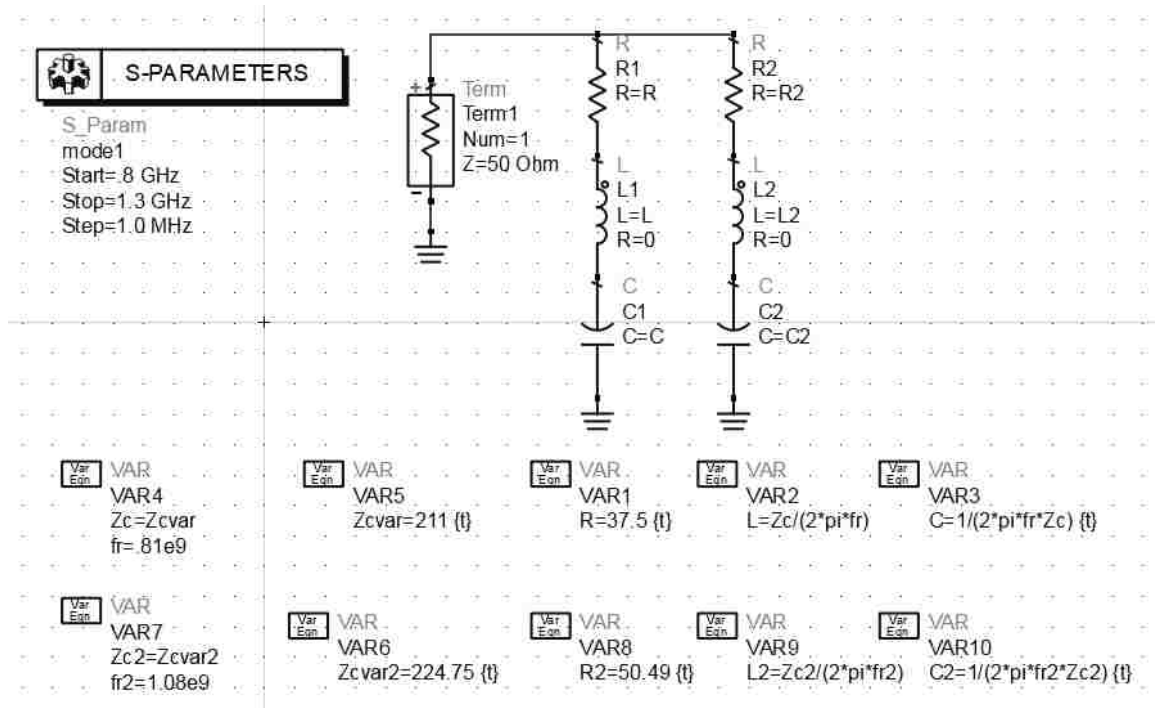


Figure 30. U-Slot Circuit Model

Changes in the overall input impedance while tuning the R and Z_c values can be observed in the Smith chart. The impedance locus of the U-slot circuit model is compared to that of the fabricated and simulated U-slot antenna (Figure 31).

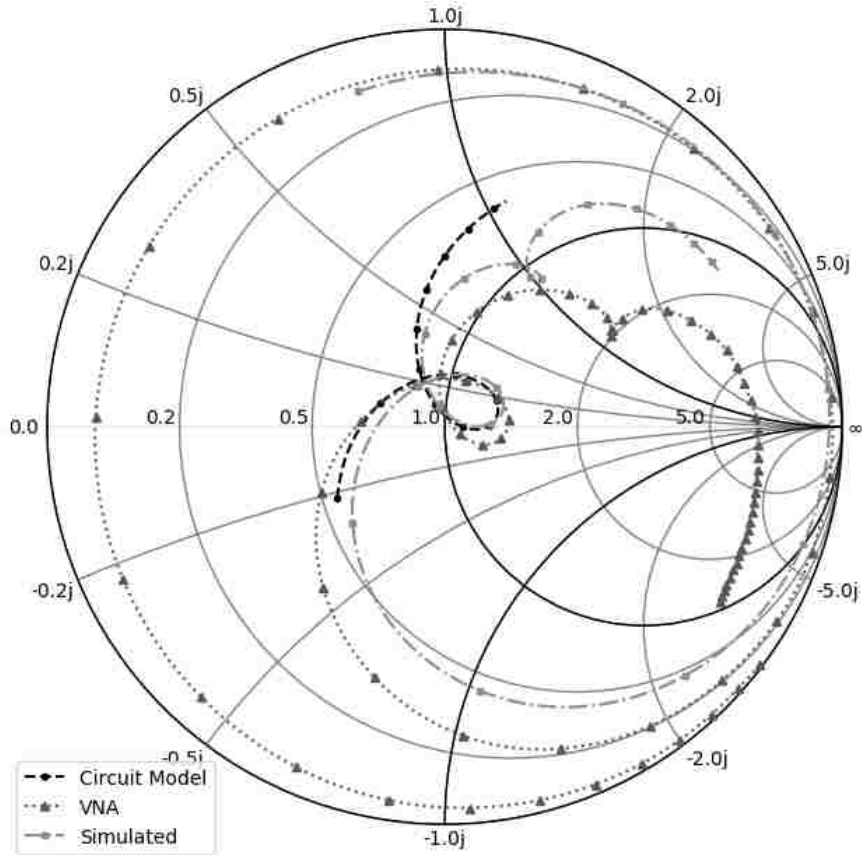


Figure 31. Comparison Between Measured & Simulated S_{11} Impedance Locus

Plots

Figure 31 shows the impedance locus of the U-slot circuit model is well in agreement with the simulation and fabricated MPA test results. It is also possible to view the impedance locus of each mode individually in the circuit model (Figure 32).

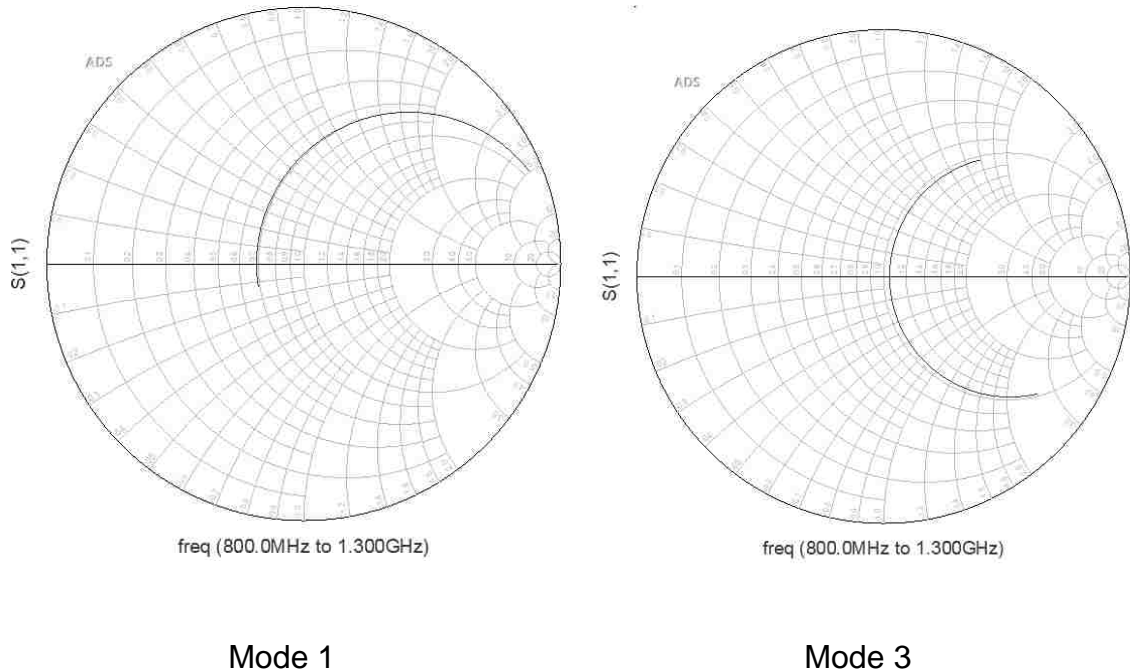


Figure 30. Circuit Model Simulated Individual Impedance Locus

The mismatch at higher frequencies in the circuit model's overall impedance locus is due to the contribution of the third, sub-resonant mode, mode 6. Mode 6 and all higher modes can be represented in the circuit model as a lumped parallel capacitance though unnecessary as the higher modes have negligible effect over the 30% bandwidth of interest. Again, it is noted that any FR4 underneath the U-slot will cause a rotation of the loop in the Smith chart. This is noticed in Figure 31 by the VNA impedance locus plot having a clockwise rotation compared to the impedance locus plot of the simulation and the circuit model. The modal Q values can be calculated from the U-slot circuit model with the following equation:

$$Q = \frac{Z_c}{R} \quad (6)$$

$$Q_1 \approx \frac{211}{38} \approx 6$$

$$Q_2 \approx \frac{225}{50} \approx 5$$

The results of which are similar to the Q values calculated from the CMA modal power distribution plots. By utilizing a circuit model of the U-slot antenna, it is demonstrated how the input impedances of the two individual resonant modes combine in parallel to form a loop in the Smith chart. At this point it is convincing that the performance characteristics of the U-slot MPA are due to the existence of modes 1 and 3. However, this does not explain the relationship between the rectangular patch, the U-slot, and the wideband characteristics. It turns out this connection can be made with coupled mode theory.

Coupled Mode Theory

Coupled Mode Theory (CMT) was introduced in the 50's however its formulation was modernized in 1991 by Haus and Huang [26]. CMT describes the characteristic behavior of a coupled system to achieve a resonant state or natural mode of vibration. This phenomenon is observed in mechanical oscillators, coupled electric circuits, molecular vibration in solids, acoustic waves, directional couplers, wave filters, and microwave amplifiers [27]. More recently,

CMT has been used to identify and improve CMA eigenvalue tracking issues [28]. According to CMT, a coupled system with two resonators will have two natural modes of vibration. The behavior of such a system can be demonstrated by the coupled pendulum system shown in Figure 33.

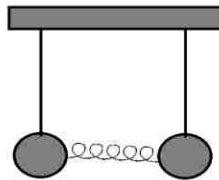


Figure 33. Coupled Pendulum System

The coupled pendulum system consists of two masses, or resonators, each hanging from a rigid support by a vertical string. In this system, the pendulums are coupled together by a horizontal spring and are capable of oscillating in one of two natural modes of vibration. That is, the pendulums will resonate in-phase at a lower natural frequency, where the spring remains un-stretched, Figure 34.

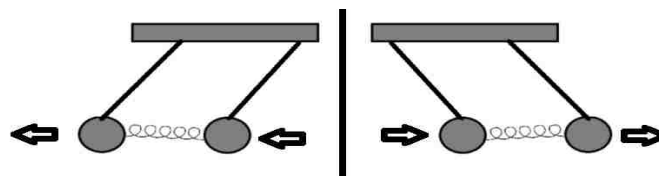


Figure 34. In-Phase Resonance

Or the pendulums will resonate out-of-phase at a higher natural frequency where the spring expands and contracts, Figure 35.

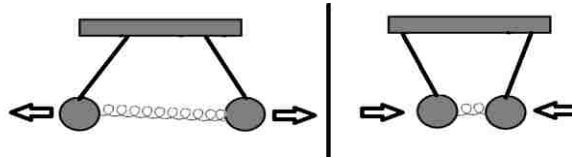


Figure 35. Out-of-Phase Resonance

Any form of motion within the coupled pendulum system can be described as the superposition of the two natural modes of oscillation. Due to symmetry, the uncoupled resonant frequency of each individual pendulum is the same; however, their coupling allows them to influence one another through the exchange of energy. Mathematically the coupled mode system is represented by equations 7 and 8 where the ω_- and ω_+ terms represent the lower and higher coupled resonant frequencies of the system and the ω_1 and ω_2 terms represent the individual uncoupled resonant frequencies of the two resonators. Lastly the K value represents the un-normalized coupling coefficient in the system.

$$\omega_- = \frac{\omega_1 + \omega_2}{2} - \sqrt{\left(\frac{\omega_1 - \omega_2}{2}\right)^2 + |K_{12}|^2} \quad (7)$$

$$\omega_+ = \frac{\omega_1 + \omega_2}{2} + \sqrt{\left(\frac{\omega_1 - \omega_2}{2}\right)^2 + |K_{12}|^2} \quad (8)$$

The above CMT equations are further described by Chuang [29] where the coupling of resonators in a system are classified as either synchronous or asynchronous (Figure 34). This designation concerns the term $\omega_1 - \omega_2$; for the synchronous case $\omega_1 - \omega_2 = 0$ and complete energy transfer from one resonator to the other is possible.

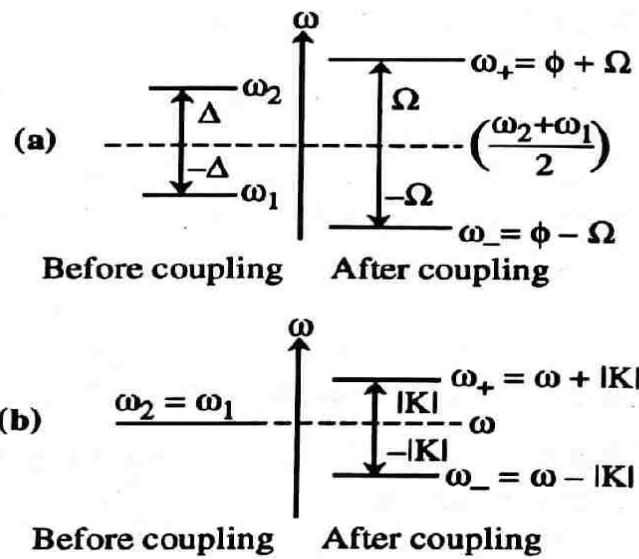


Figure 36. a) Asynchronous Coupling, b) Synchronous Coupling [29]

Regardless of the coupling type or the individual uncoupled resonator frequencies, a coupled system will exhibit a lower, in-phase resonant frequency

and a higher, out-of-phase resonant frequency. At this point one might ask, what does CMT have to do with wideband U-slot MPA behavior?

Recall the two resonant modes 1 and 3 from the previous CMA analysis. Mode 1 was resonant at a frequency of 0.81 GHz and mode 3 was resonant at a frequency of 1.08 GHz. Due to the nature of the U-slot MPA, modal current plots prove too complex for use when it comes to observing the relationship between the patch and the U-slot. However, if we observe the charge distributions in modes 1 and 3 from the CMA results, identifying an in-phase and out-of-phase coupling between the U-slot and the rectangular patch is possible. The CMA charge distributions of modes 1 and 3 are pictured below in Figure 37 where shades of white represent negative charge and shades of black represent positive charge.

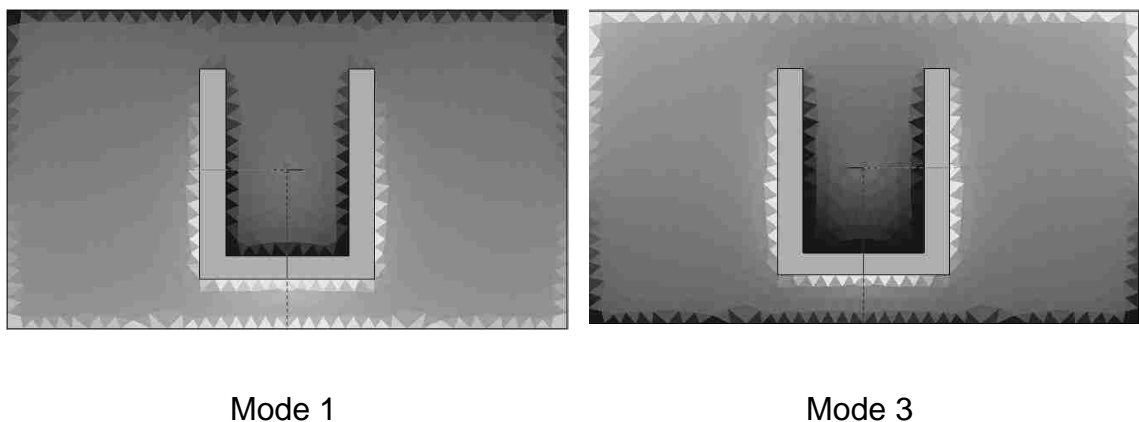


Figure 37. CMA Charge Distributions

The charge distributions of mode 1, Figure 37a, show that the rectangular patch's horizontal edges and the horizontal portion of the U-slot's edges have an in-phase charge distribution at the lower resonant frequency of 0.81 GHz. The charge distributions of mode 3, Figure 37b, show that the rectangular patch's horizontal edges and the horizontal portion of the U-slot's edges have an out-of-phase charge distribution at the higher resonant frequency of 1.08 GHz. In accordance to CMT, the resonant frequency of mode 1 and mode 3 appear to be the in-phase and out-of-phase frequencies resulting from the coupling between the patch and the U-slot. It would then follow that the uncoupled individual resonant frequencies of the rectangular patch and the U-slot should fall in between the lower and higher coupled resonant frequencies, around 0.95 GHz corresponding to the un-normalized coupling coefficient. It is possible to determine the uncoupled resonant frequency of the rectangular patch by simply removing the U-slot from the previous CMA simulation. The resulting eigenvalues of which are plotted in Figure 38.

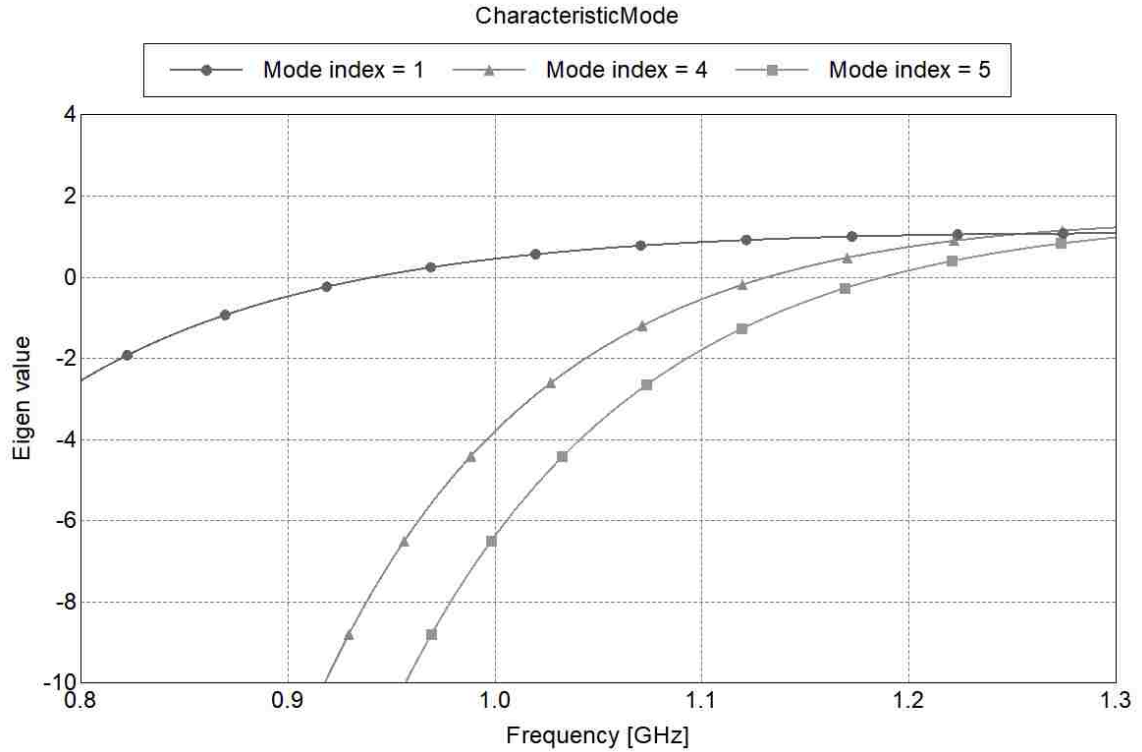


Figure 38. Eigenvalues of Rectangular Patch Without the U-Slot

As predicted by CMT, the first resonant mode of the rectangular patch without the U-slot appears at 0.95 GHz. To verify that the first resonant mode is the correct patch mode, its near and far-field radiation patterns are examined (Figure 39).

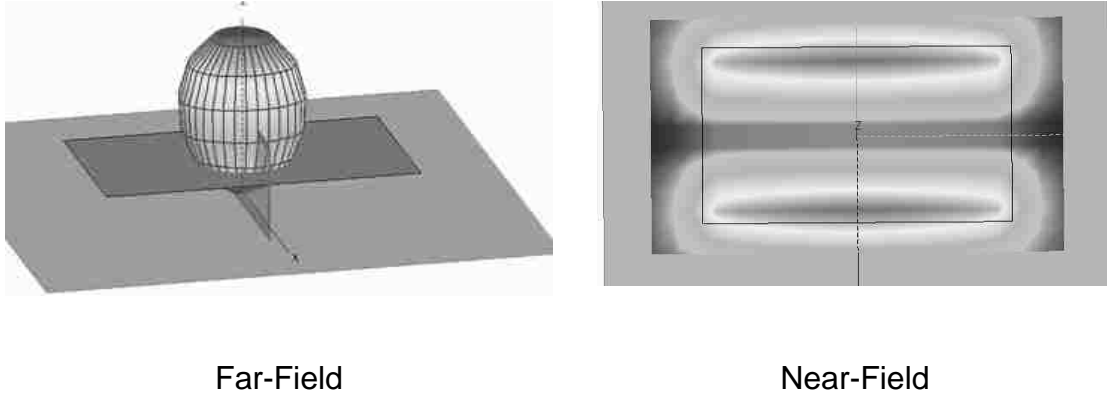


Figure 39. Field Patterns of Rectangular Patch Without the U-Slot

The results in Figure 39 confirm the proper patch mode radiates at 0.95 GHz.

The U-slot has been analyzed using the duality relationship between a slot resonator and a dipole [16]. This duality is often referred to as Babinet's principle, which was translated into terms of antenna analysis by Booker [30]. While the former publications are useful, a method for determining the uncoupled resonance of the U-slot requires further investigation although expected to be around 0.95 GHz according to CMT. If the uncoupled frequency of the U-slot resonator was not the same or close to 0.95 GHz the coupled behavior would not be observed.

With the uncoupled resonant frequency of the rectangular patch and the two resonant CMA modes, it is possible to calculate the un-normalized coupling

coefficient between the patch and U-slot resonators from the equations in Figure 36 as shown below,

$$\omega_+ = \omega + |K| \Rightarrow 1.08 = .95 + K \Rightarrow K = 0.13 \text{ rads/s}$$

$$\omega_- = \omega - |K| \Rightarrow .82 = .95 - K \Rightarrow K = 0.13 \text{ rads/s}$$

The relationship between wideband behavior, CMA, and CMT is summarized in Figure 40.




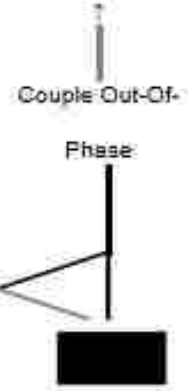
30% Bandwidth & Loop in the Smith Chart		
Combined Modal Input Impedances:		
CMA	Mode 1 $f_r = 0.82 \text{ GHz}$	Mode 3 $f_r = 1.02 \text{ GHz}$
CMT	 U-Slot resonator $f_r = 0.95 \text{ GHz}$	 Patch Resonator $f_r = 0.95 \text{ GHz}$

Figure 40. Relationship Between CMA, CMT, and Wide Bandwidth

Starting at the bottom of Figure 40, the individual rectangular patch and U-slot resonators are depicted with their uncoupled resonant frequencies in the CMT analysis level. Due to the coupling in the system, these two individual resonators

will combine in-phase resulting in a lower resonate frequency and an out-of-phase higher resonate frequency. These two coupled lower and higher resonant frequencies are the resonant frequencies of mode 1 and 3 identified in the CMA simulation. Finally, the combined input impedances of mode 1 and mode 3 result in a loop in the Smith chart, shown with the circuit model, causing the wideband behavior observed at the driven analysis level. While attributing the wideband performance of the U-slot antenna to the existence of two resonators is correct, it should not be assumed that the nulls observed in the S_{11} log magnitude plot are the resonant frequencies of the rectangular patch and the U-slot. In general, these nulls do not correspond to the resonant frequencies of the relevant characteristic modes. Therefore, S_{11} log magnitude nulls are of little importance when it comes to designing U-slot MPAs for broadband use. This non-relationship is made apparent in Figure 41.

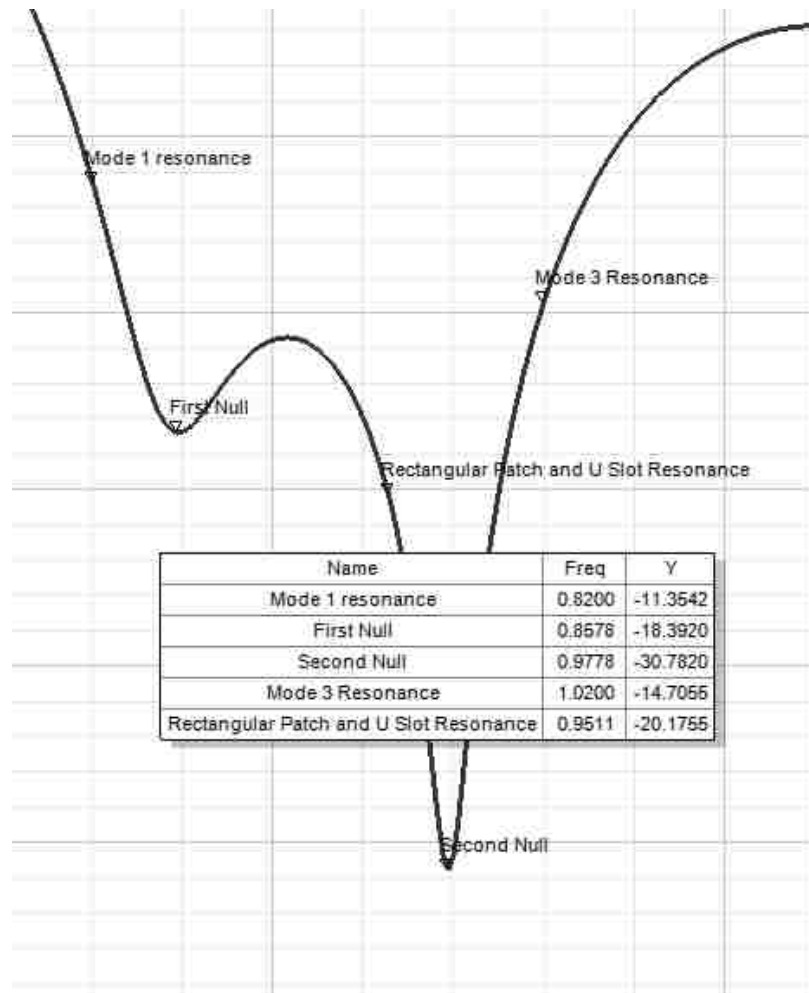


Figure 41. S_{11} Log Magnitude Plot

Figure 41 demonstrates that the different characteristic resonances of the U-slot MPA do not share frequencies with the observed null locations.

Chapter 3

Experimentation & U-Slot Design Methodology

Designing a 2.5 GHz U-Slot MPA

By understanding the behavior of the U-slot MPA at its fundamental level, it is possible to create a design method based upon the wideband causalities. This will not only benefit antenna designers but also provide further evidence of the theory presented in the previous section. To exercise the design method, a center frequency of 2.5 GHz is selected along with a 3/8" thick (0.1λ) Teflon substrate ($\epsilon_r = 2.2$). The U-slot MPA will be center fed with a SMA coaxial probe having a feed pin diameter of 0.05". According to CMT, the center frequency of 2.5 GHz will be the uncoupled resonant frequency of the rectangular patch and the U-slot resonator. Therefore, the first step in the design process will be to create a rectangular patch, on a 3/8" thick Teflon substrate, whose TM_{10} mode appears near 2.5 GHz. The starting dimensions of which will be of the same wavelength percentage of the original U-slot MPA; ($L \approx 0.7\lambda$, $W \approx 0.4\lambda$). Since CMA will be required to show the operational characteristic of the 2.5 GHz U-slot MPA, much of the design process will be conducted in Feko and later refined in HFSS before fabrication. The 2.5 GHz rectangular MPA model, dimensions, and CMA results are shown in Figure 42 and 43 after tuning.

Length = 2"

Width = 1.3"

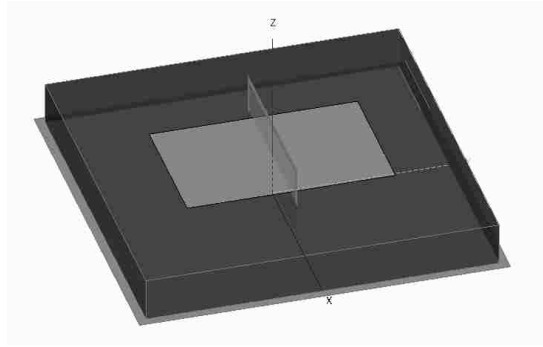


Figure 42. 2.5 GHz Rectangular Patch

Note: Since CMA is excitation-less, including the coax center feed pin is not required at this stage. In addition, dielectrics are defined as infinite in CMA simulations.

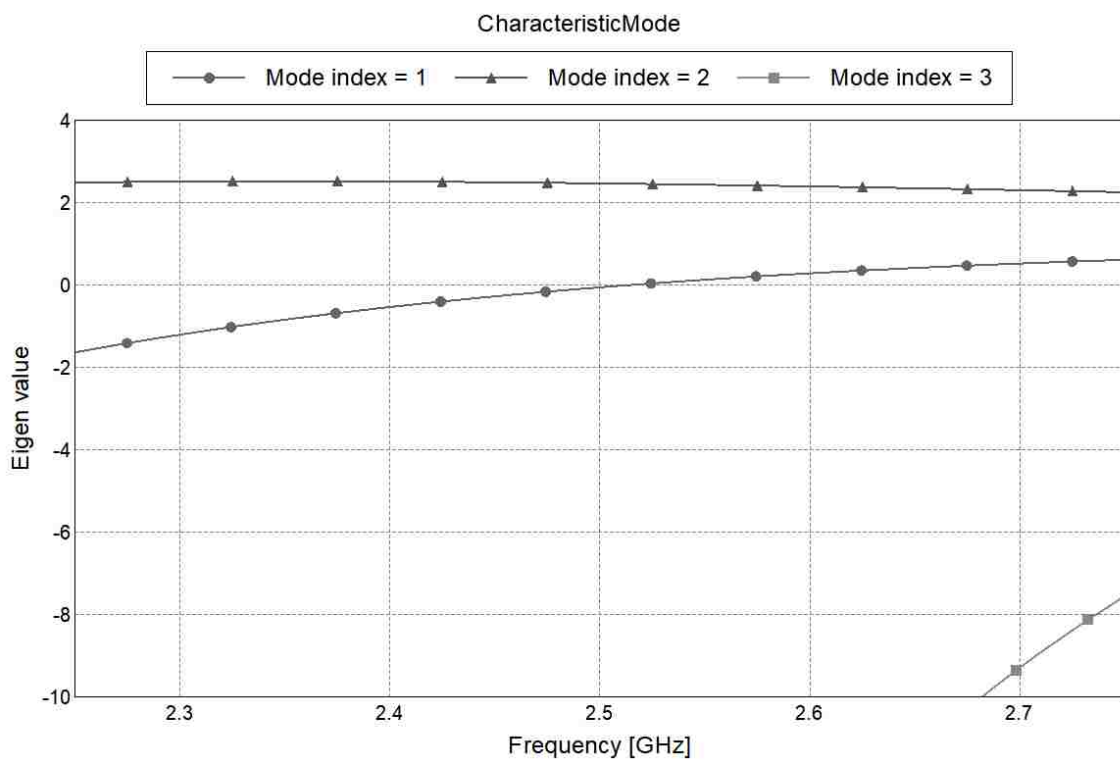


Figure 43. Eigenvalue Plots of 2.5 GHz Rectangular Patch

From the eigenvalue plots in Figure 43, it is observed that the rectangular patch has a resonant mode near 2.5 GHz. It is necessary to verify this is the proper patch mode by analyzing the mode's near and far-field patterns (Figure 44).

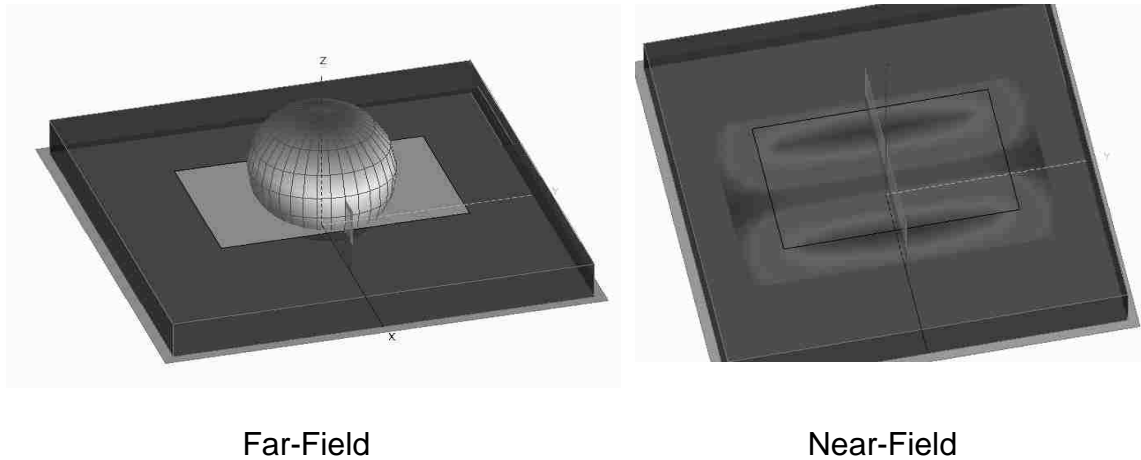


Figure 44. 2.5 GHz Rectangular Patch Radiation Patterns

Confirming the desired patch mode is resonant around 2.5 GHz, the second step is to add the U-slot resonator to the patch. As a starting point, the slot's vertical portions can be set to 0.25λ and the horizontal portion can be set to 0.2λ with their widths being 0.03λ . The U-slot and coaxial feed pin location can be centered on the rectangular patch as a starting point. The initial design of the 2.5 GHz U-slot MPA is shown in Figure 45.

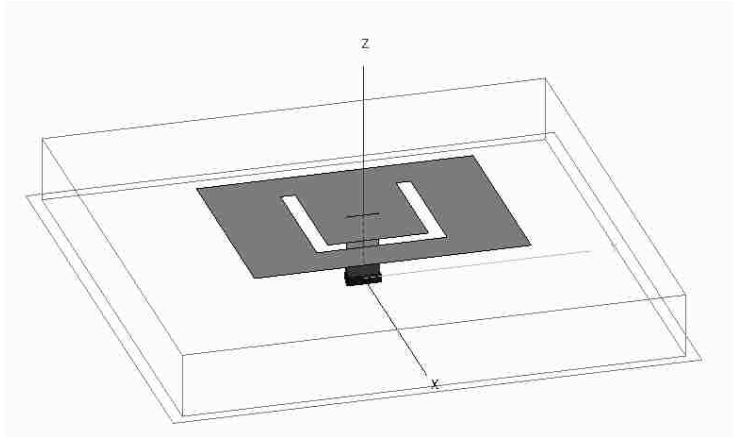


Figure 45. 2.5 GHz U-Slot Model

At this point it is necessary to include the feed pin which can be modeled by a rectangular strip whose width is four times the diameter of the coaxial feed pin. With the addition of the U-slot resonator, CMT predicts the observation of in-phase, lower, and out-of-phase, higher, resonant modes resulting from the coupling between the patch and the U-slot. In the next step, driven and CMA simulation will be conducted at the same time throughout what will be the initial U-slot tuning phase. During this process the focus will be on achieving the proper loop in the Smith chart with the driven simulation while the CMA simulation will provide verification of the predicted results and proper modal behaviors for wideband operation. The following table summarizes the various “tuning knobs” available for centering the loop in the Smith chart.

		Resulting Change in the Loop on the Smith Chart					
		Larger	Smaller	Clock left	Clock right	Move Left	Move Right
Fine Tuning Knobs	U Slot Length	↑	↓	↑	↓		
	Patch Length	↓	↑	↓	↑		
	Patch Width			↓	↑	↓	↑
	U Slot Position					↓	↑
Course Tuning Knobs	Feed Position	↓	↑	↑	↓		
	Substrate Height	↓	↑			↓	↑

Table 1. Impedance Loop Tuning Table

For wideband performance the goal is to maximize the size of the loop in the Smith chart while remaining inside the $VSWR = 2$ circle. By referencing Table 1,

adjustments to the “Tuning Knobs” are shown by upward pointing arrows signifying an increase in size or position, or a downward pointing arrow signifying a decrease in size or position. The effect on the loop in the Smith chart from these adjustments is stated at the top of each column. Care should be taken when the bandwidth appears beyond 30% as a wider bandwidth can result from the excitation of a third, sub-resonant mode whose radiation pattern is undesirable. The eigenvalue results from adding the U-slot to the rectangular patch and tuning using Table 1 are shown in Figure 46.

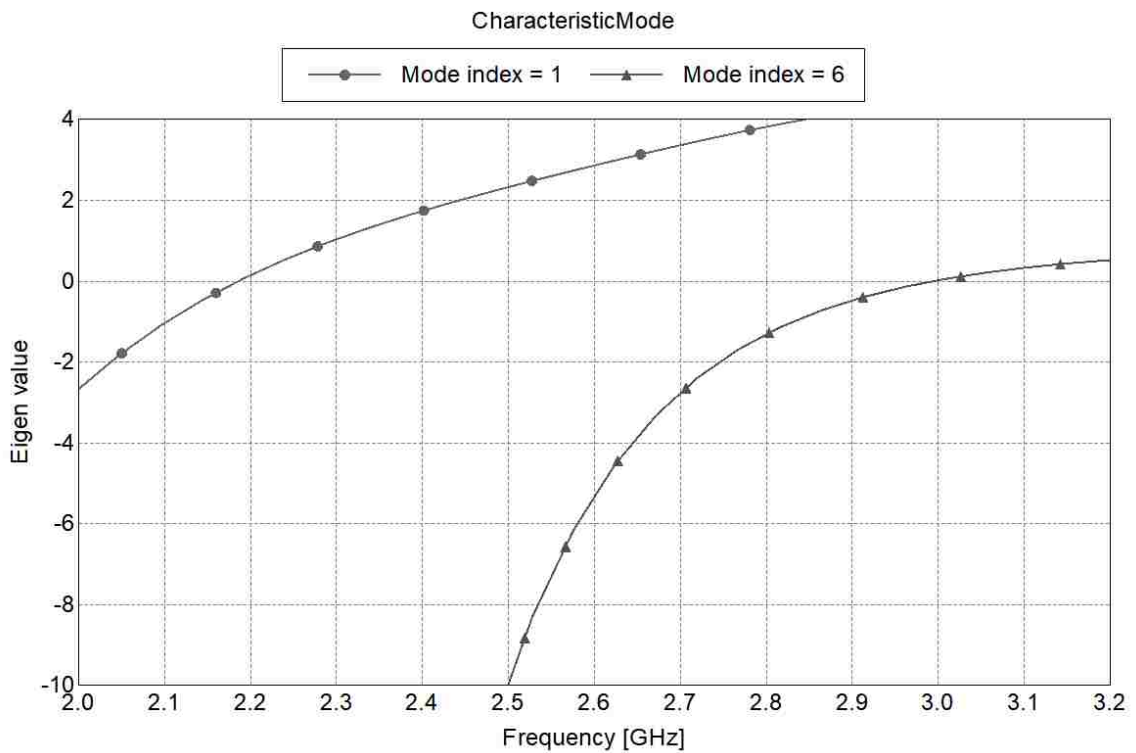


Figure 46. Eigenvalue Plots of 2.5 GHz U-Slot MPA

The results from Figure 44 show that two resonant modes, 1 and 6, appear around 2.2 and 3 GHz. To verify mode 1 and 6 are the desired modes, it is

necessary to observe their characteristics beginning with the near and far-field patterns (Figures 47 and 48).

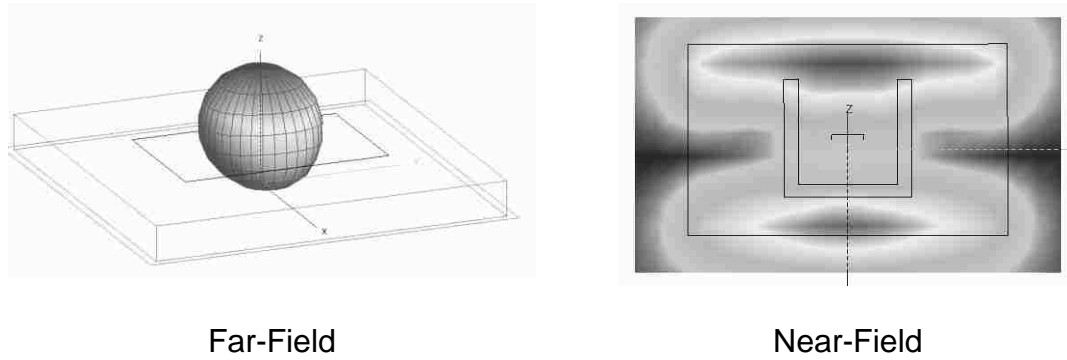


Figure 47. Field Results for Mode 1

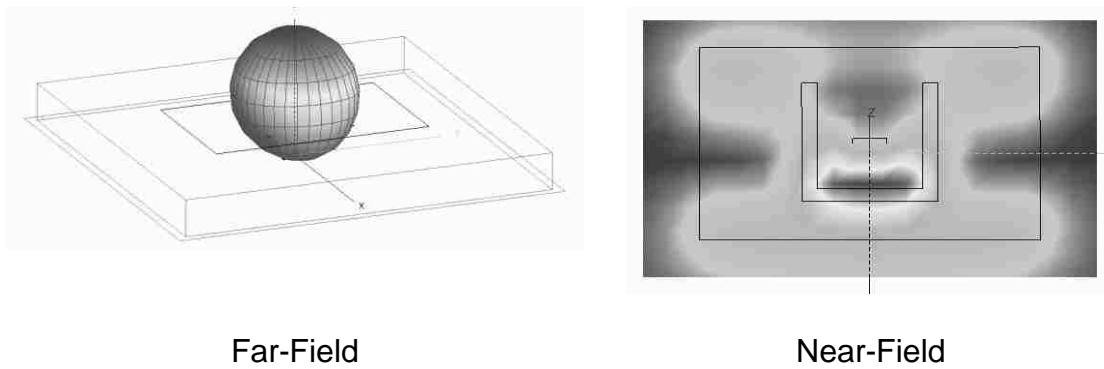


Figure 48. Field Results for Mode 6

The near and far-field results for modes 1 and 6 confirm they are the desired U-slot MPA modes and have a stable radiation pattern over the 30% bandwidth.

The impedance locus for both modes is displayed in Figure 49.

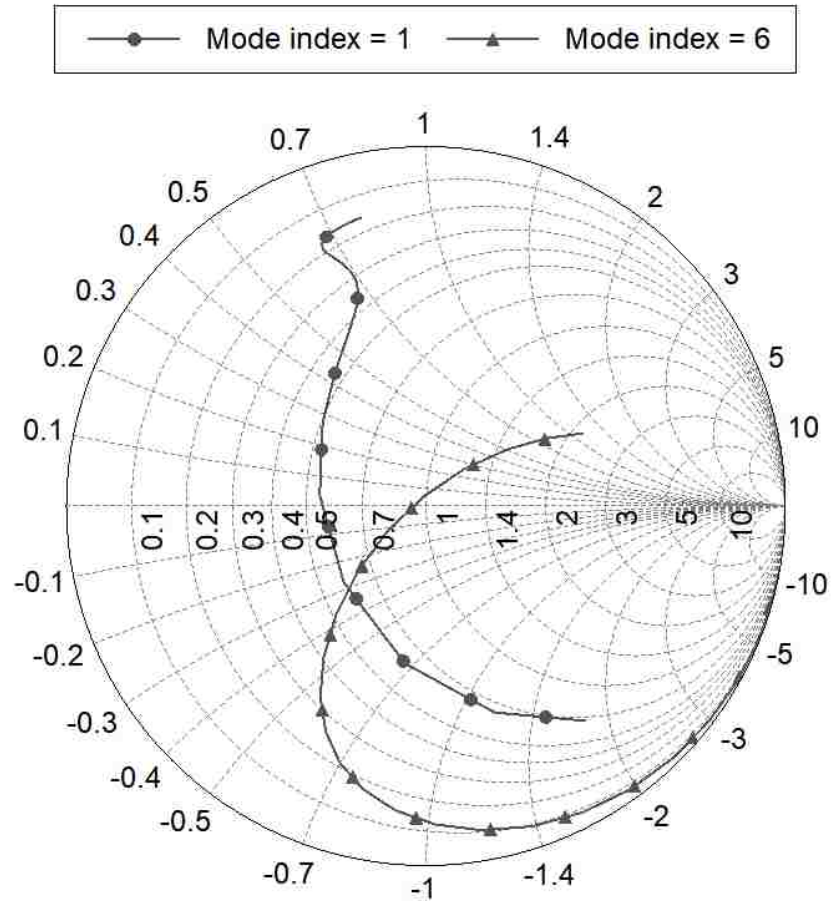


Figure 49. Impedances Locus of Mode 1 & 6

The modal impedance plots in Figure 49 show a similar behavior to the modal impedance plots of the original U-slot MPA and their combined impedances are expected to result in a loop in the Smith chart as well. The modal power plots for mode 1 and 6 are shown in Figure 50.

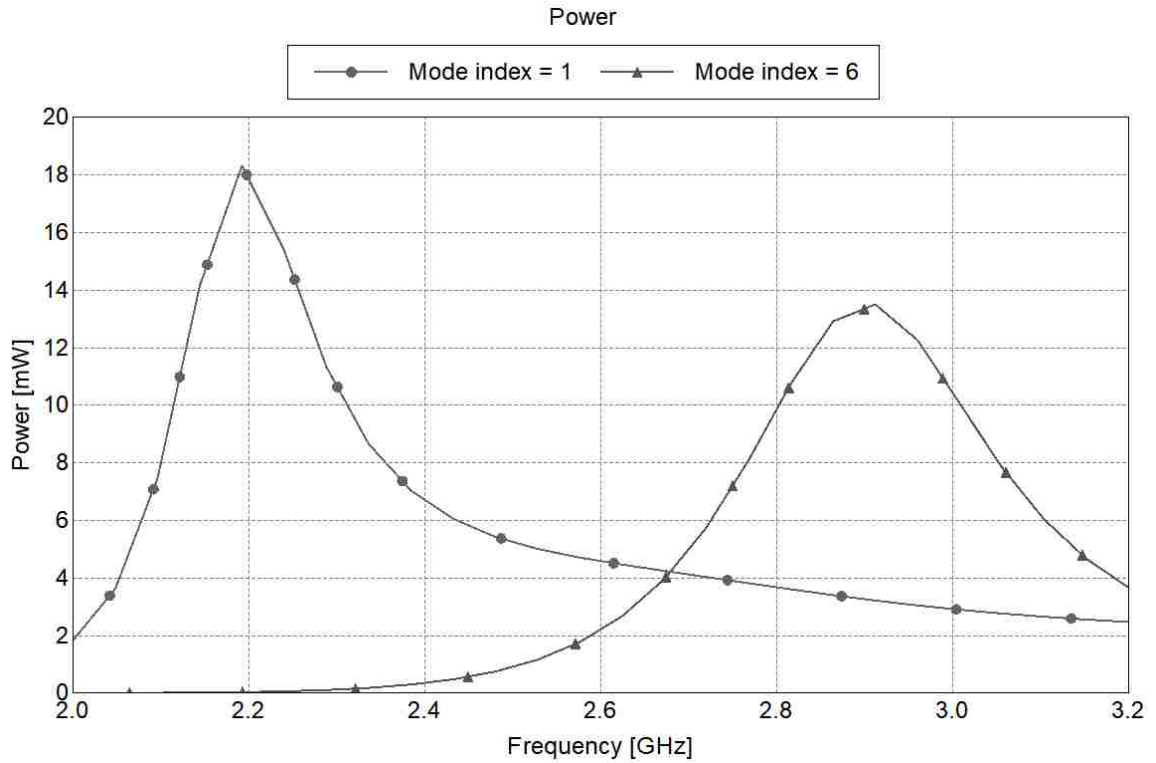
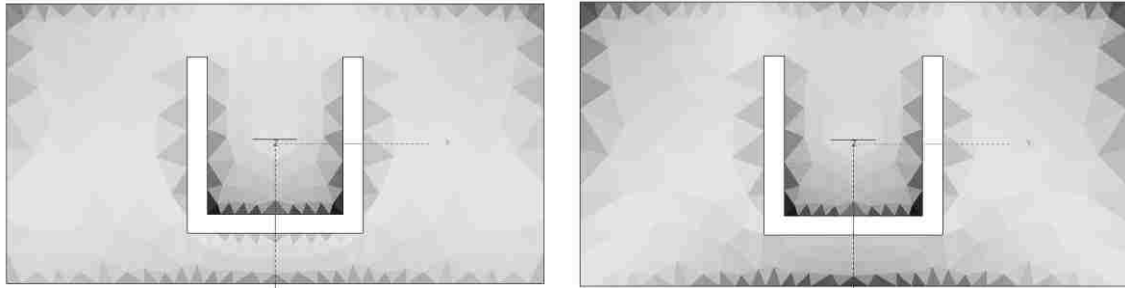


Figure 50. Modal Power Plot of 2.5 GHz U-Slot MPA

The modal power plots of Figure 50 correspond to a Q of about 10 for each mode. Lastly, the charge distributions of modes 1 and 6 for the 2.5 GHz U-slot MPA are shown in Figure 51 confirming the in-phase and out-of-phase relationship between the rectangular patch and U-slot resonators.



Mode 1

Mode 6

Figure 51. Modal Charge Distributions

While not as obvious as in the original U-slot design, the in-phase and out-of-phase charge distribution is still observed between the rectangular patch and the U-slot at the two resonant frequencies. This will become more obvious as the design is tuned further. Lastly, the driven results for the initial 2.5 GHz U-slot MPA design are displayed in Figure 52 and 53.

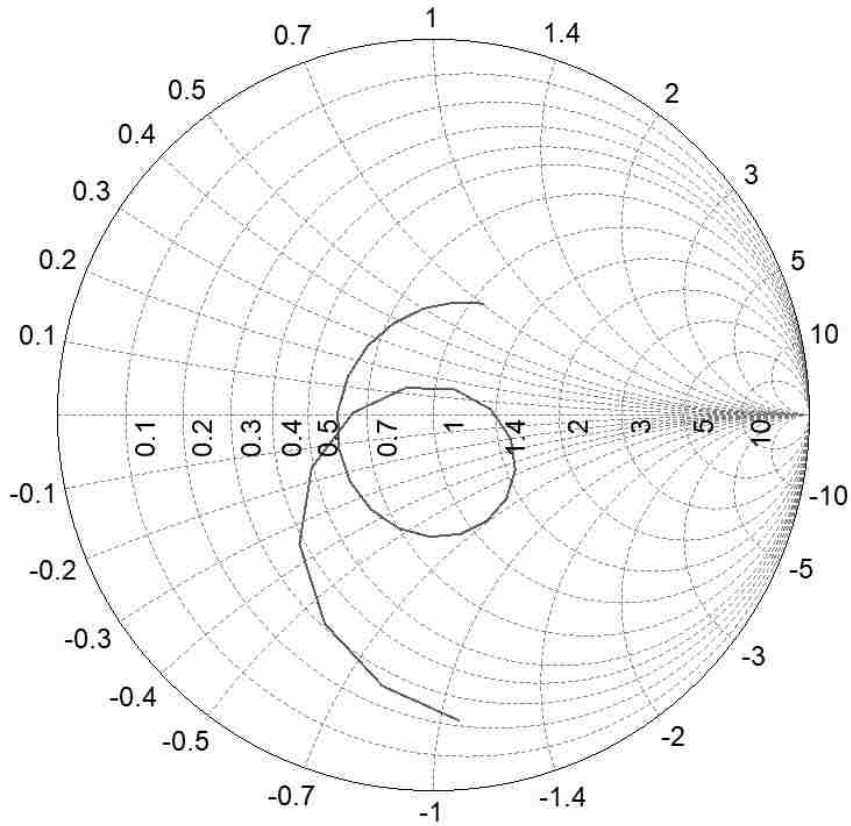


Figure 52. Simulated S_{11} Impedance Locus

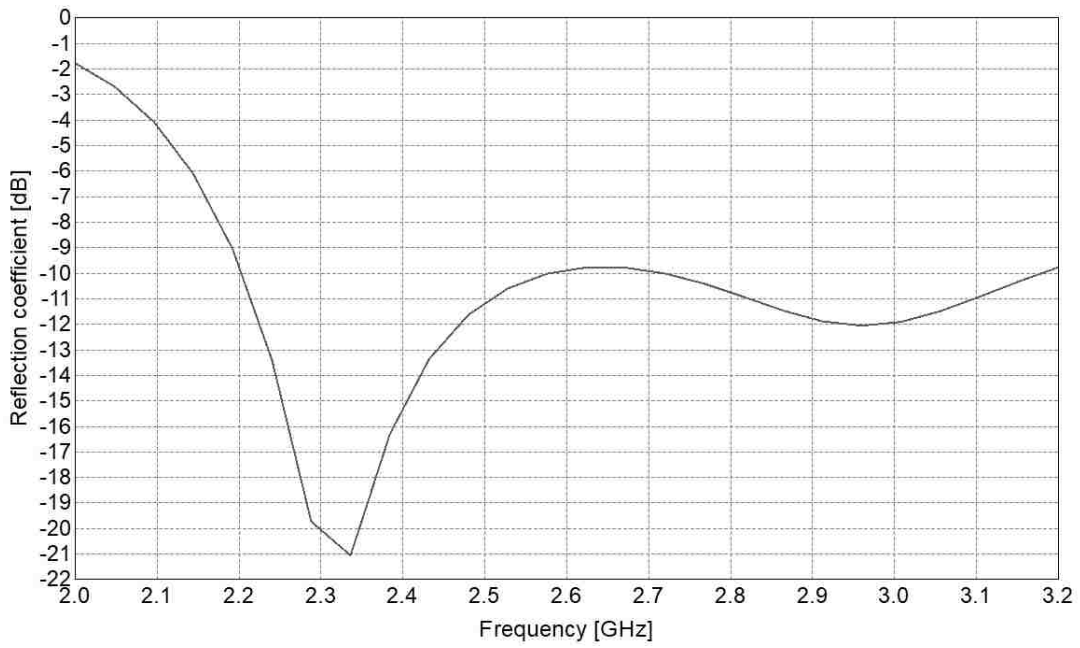


Figure 53. Simulated S_{11} Log Magnitude

The U-slot circuit model can be created for the 2.5 GHz U-slot MPA as seen in Figure 54.

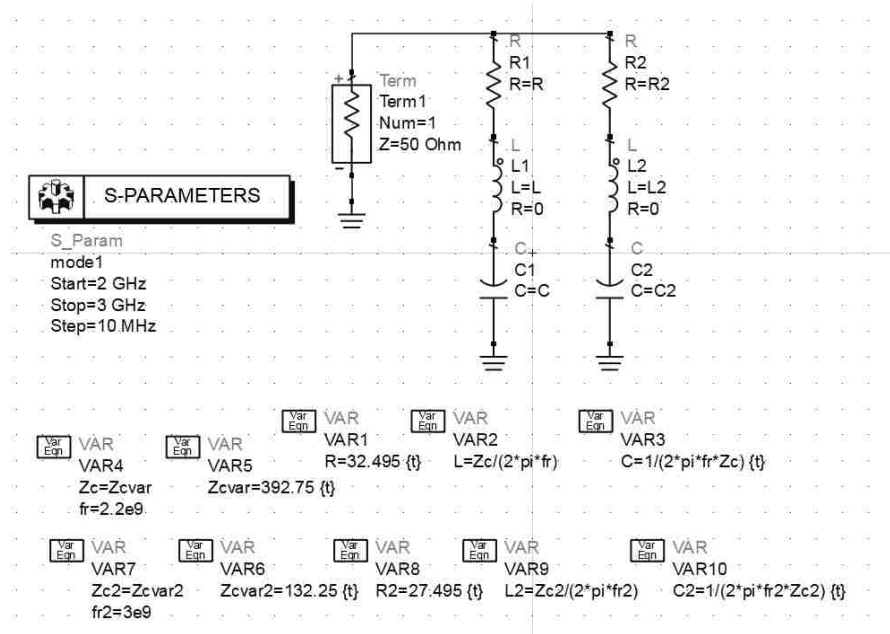


Figure 54. 2.5 GHz U-Slot MPA Circuit Model

The component values in Figure 54 result in a Q of about 12 and 5. The individual modal impedances and their combination is shown in Figure 55.

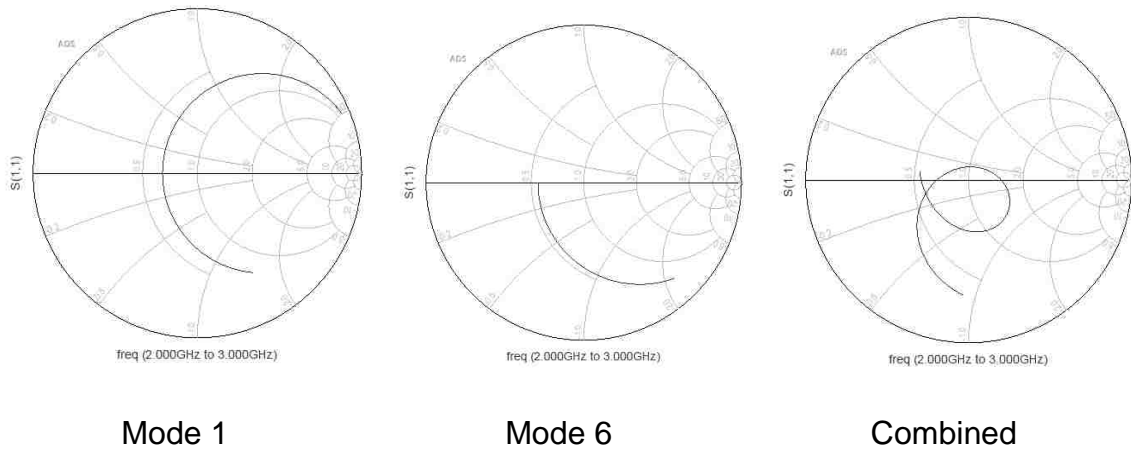


Figure 55. Simulated Impedance Locus of 2.5 GHZ U-Slot MPA Circuit Model

At this point the basic operation, characteristics, and dimensions of the U-slot design are confirmed. The expected, CMA, circuit model, and driven results are summarized in Table 2.

Results	Center Frequency	In-Phase Coupled Frequency	Out-Of-Phase Coupled Frequency	Bandwidth	K	Q
Expected	2.5 GHz			30%		
CMA		2.2 GHz	3 GHz		0.4	10
Driven	2.67 GHz			35%		
Circuit Model						12 & 5

Table 2. Expected, CMA, and Driven Results

With the verification of the basic wideband U-slot principles at work, the 2.5 GHz U-slot design will be finalized in HFSS where a higher level of fidelity can be incorporated. This includes a 62-mil FR4 backing, a 6" x 6" x 3/8" Teflon

substrate, a circular feed pin, and a 12" diameter circular ground plane. All factors of which that are not accounted for in the CMA simulations. Differences between the HFSS and Feko simulations are expected and additional tuning will be required to account for the increased fidelity. The HFSS 2.5 GHz U-slot MPA model is shown in Figure 56.

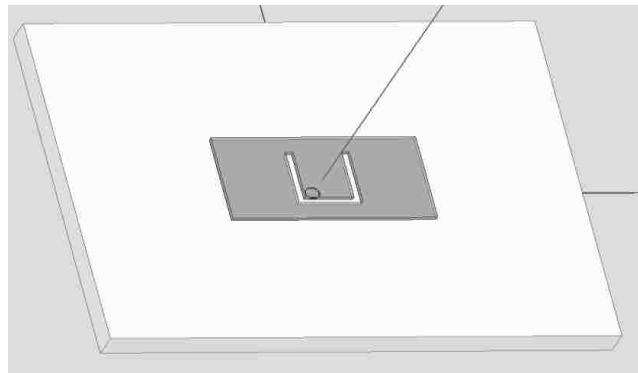


Figure 56. 2.5 GHz U-Slot HFSS Model

To account for differences in performance resulting from the increased fidelity, the same tuning table used in the initial design can be utilized to reposition the impedance locus loop in the $VSWR = 2$ circle on the Smith chart. The HFSS results after tuning are displayed in Figure 57 through 59.

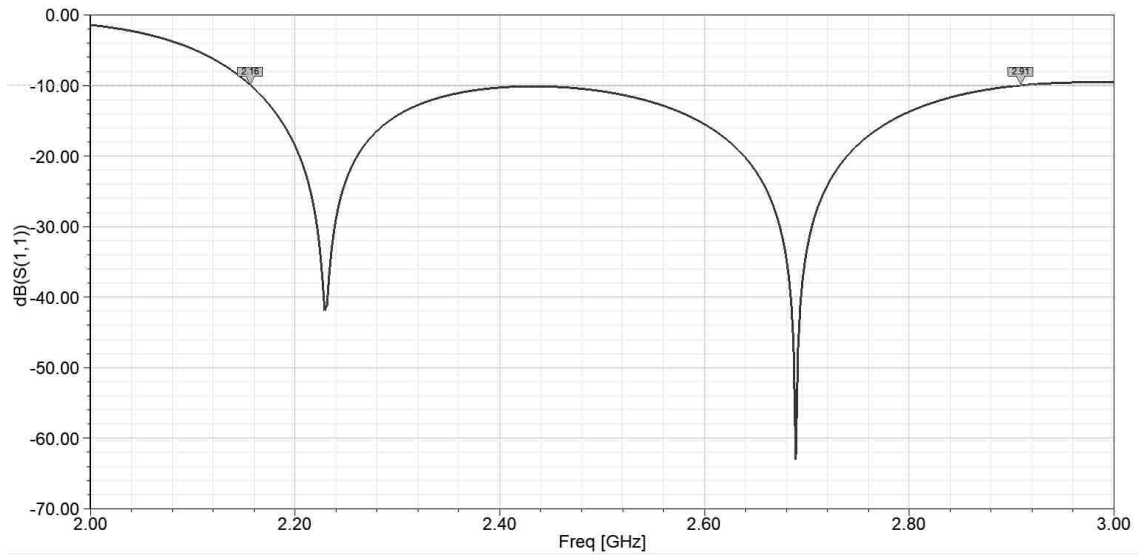


Figure 57. Simulated 2.5 GHz U-Slot S_{11} Log Magnitude

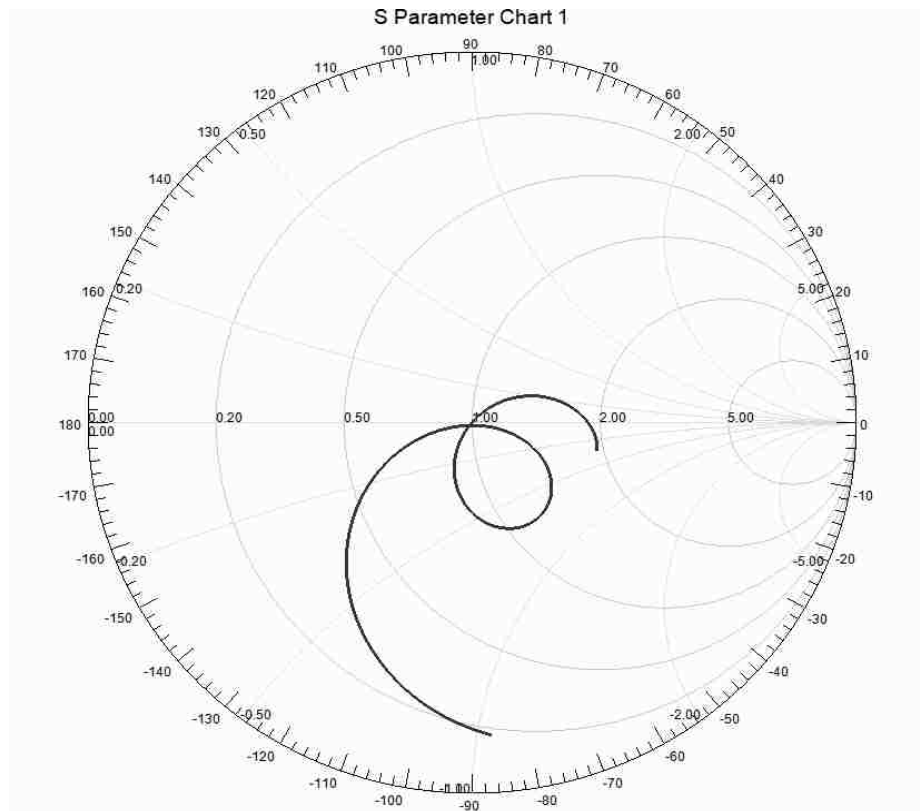


Figure 58. Simulated S_{11} Impedance Locus

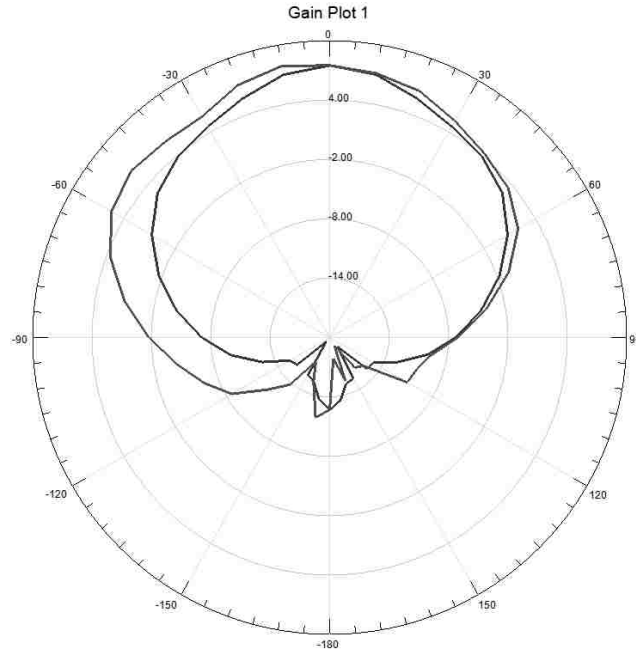
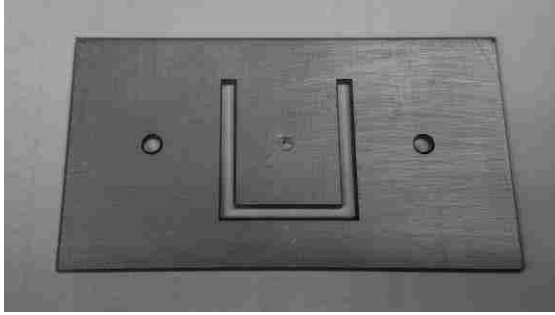
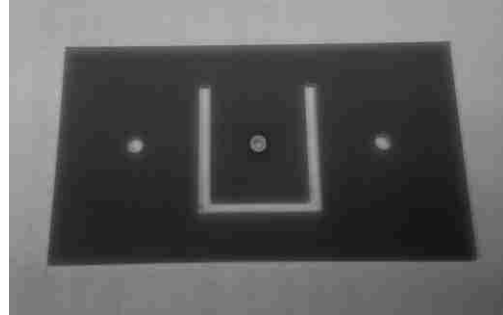


Figure 59. Simulated Gain (dB) in the x-z & y-z Planes

The results of Figures 57 through 59 verify the 2.5 GHz U-slot MPA has a wide bandwidth while confirming the operational characteristics. With the satisfactory simulation results, fabricating the 2.5 GHz U-slot MPA design is now possible (Figure 60). The fabricated 2.5 GHz U-slot MPA on FR4 was mounted to the Teflon substrate and a 12" diameter circular ground plane with nylon screws.



Side 1 (Metallization)



Side 2 (FR4)

Figure 60. Fabricated 2.5 GHz U-Slot MPA

Nylon screws were also added to the edges of the Teflon to reduce any air gaps between the ground plane and the Teflon substrate. The completed test assembly is shown in Figure 61.

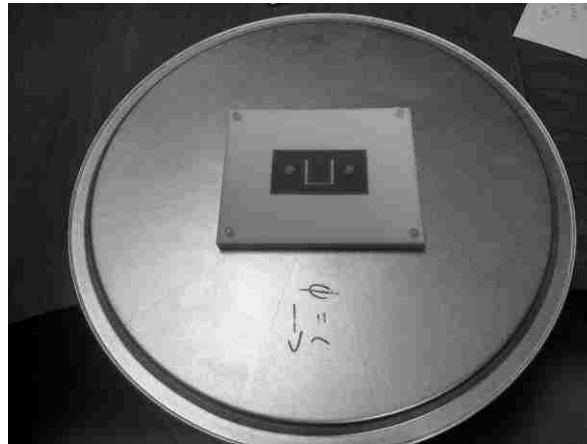


Figure 61. 2.5 GHz U-Slot MPA Complete Test Assembly

The above assembly was then tested using the Satimo chamber and the FieldFox VNA in an anechoic chamber (Figure 62 and 63).

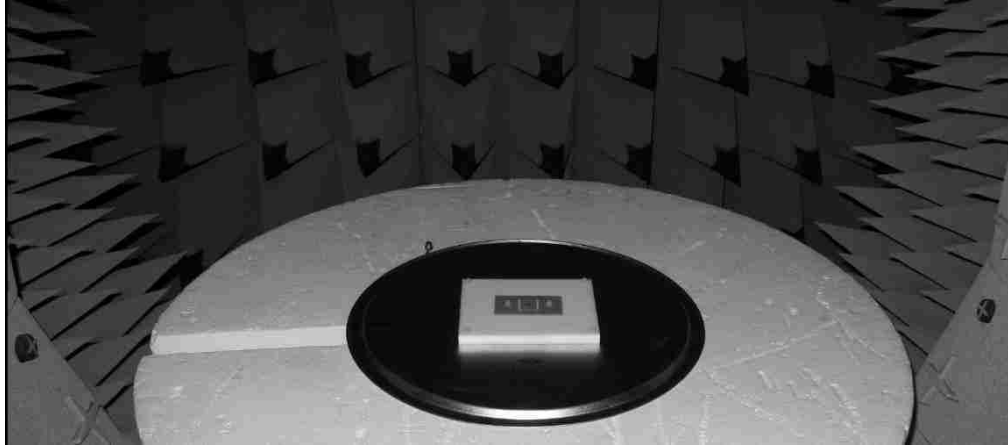


Figure 62. 2.5 GHz U-Slot MPA Test in Satimo Chamber

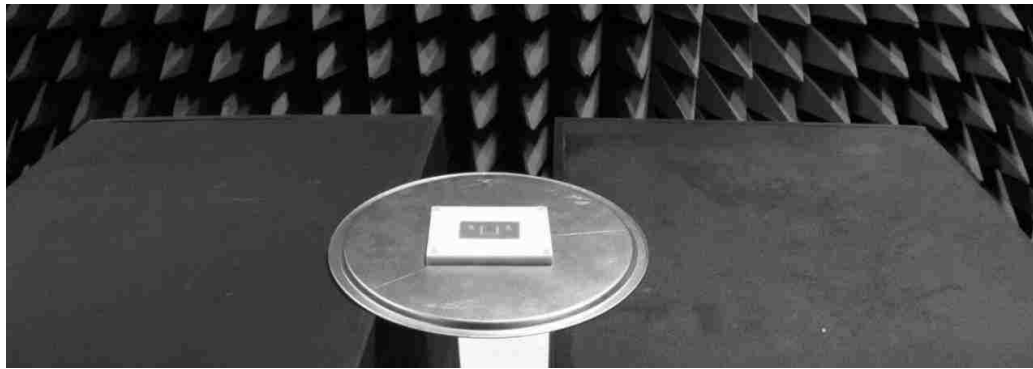


Figure 63. 2.5 GHz U-Slot MPA Test with VNA In Anechoic Chamber

The test results of which are shown in Figures 64 through 69.

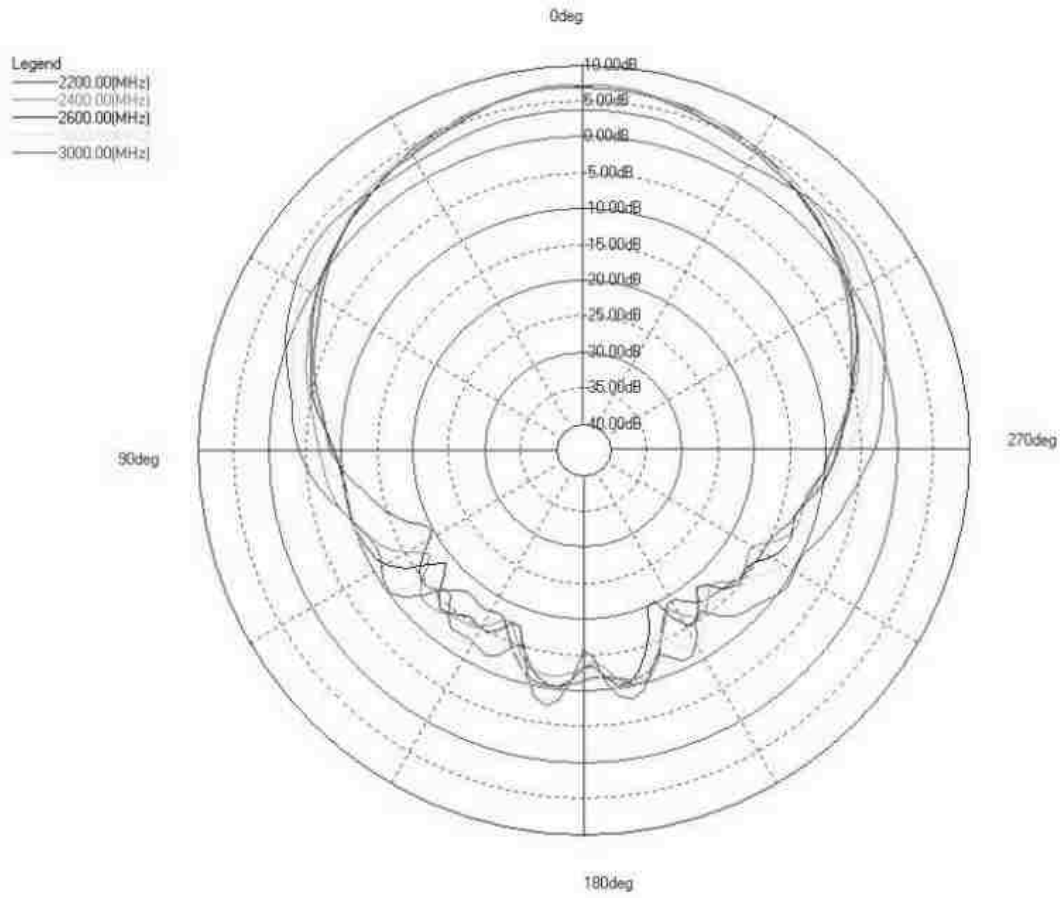


Figure 64. Measured Satimo Far-Field Results View 1

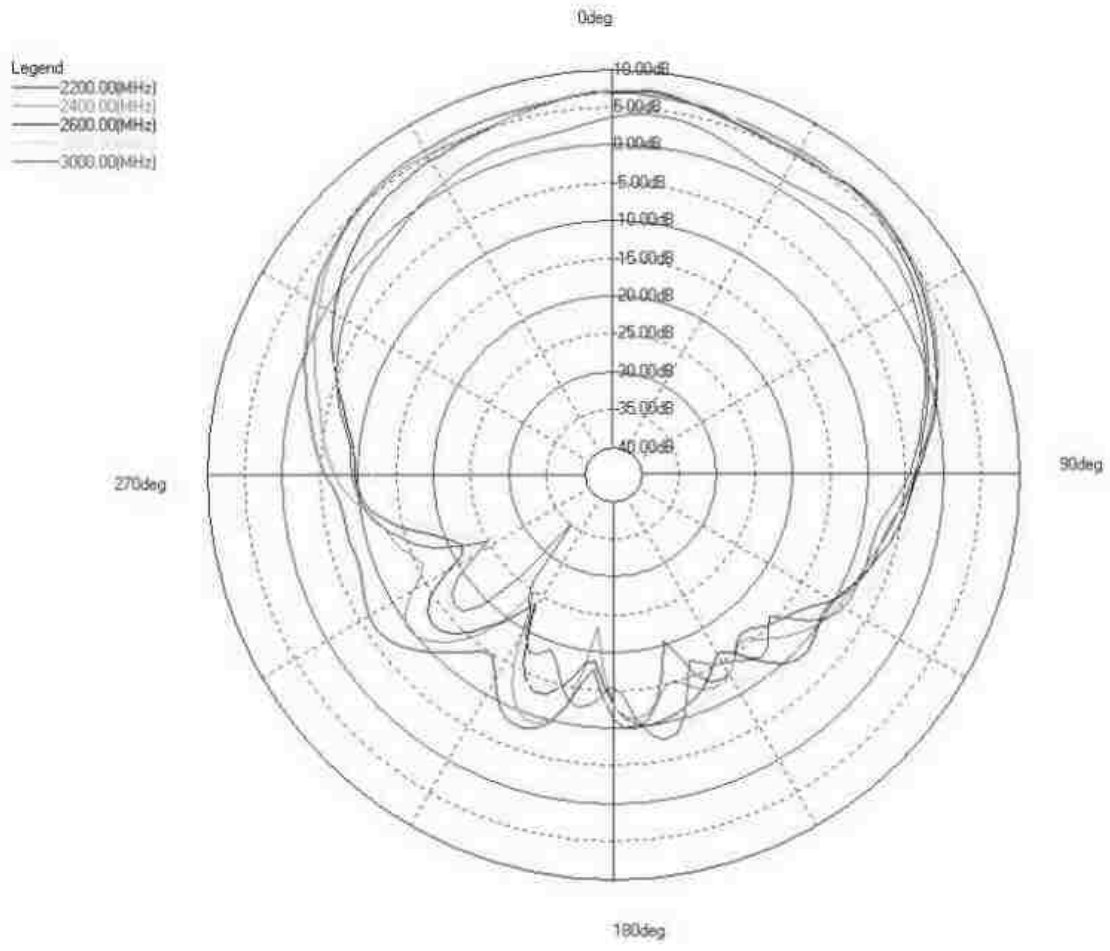


Figure 65. Measured Satimo Far-Field Results View 2

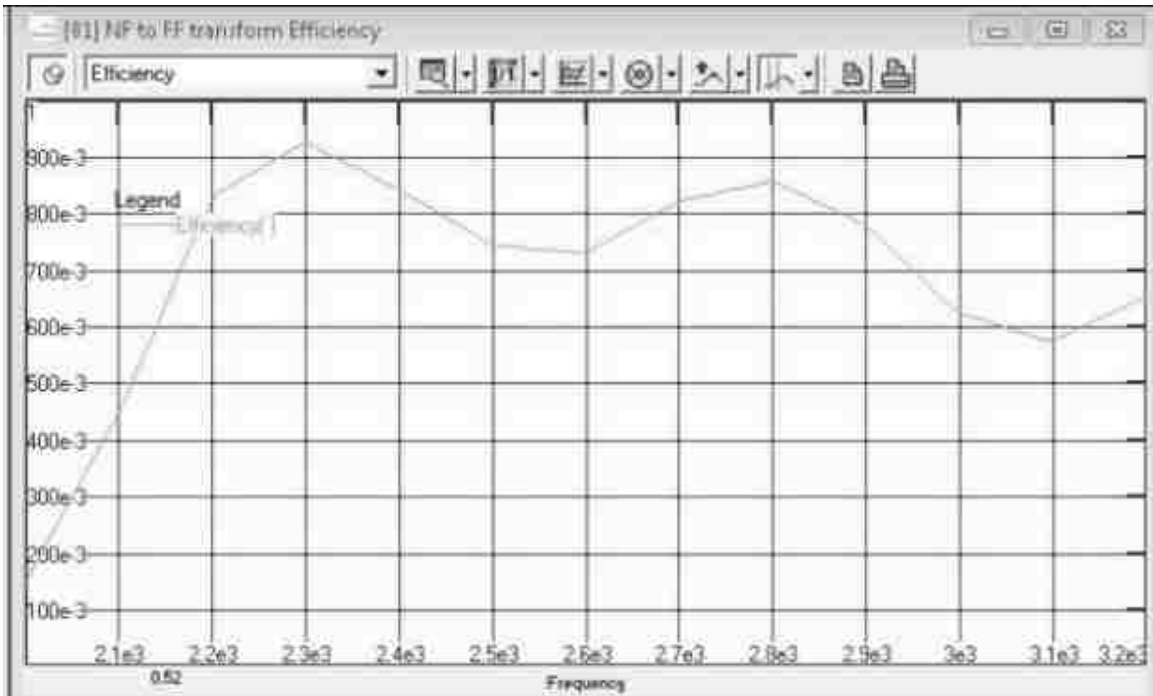


Figure 66. Measured Satimo Efficiency Results

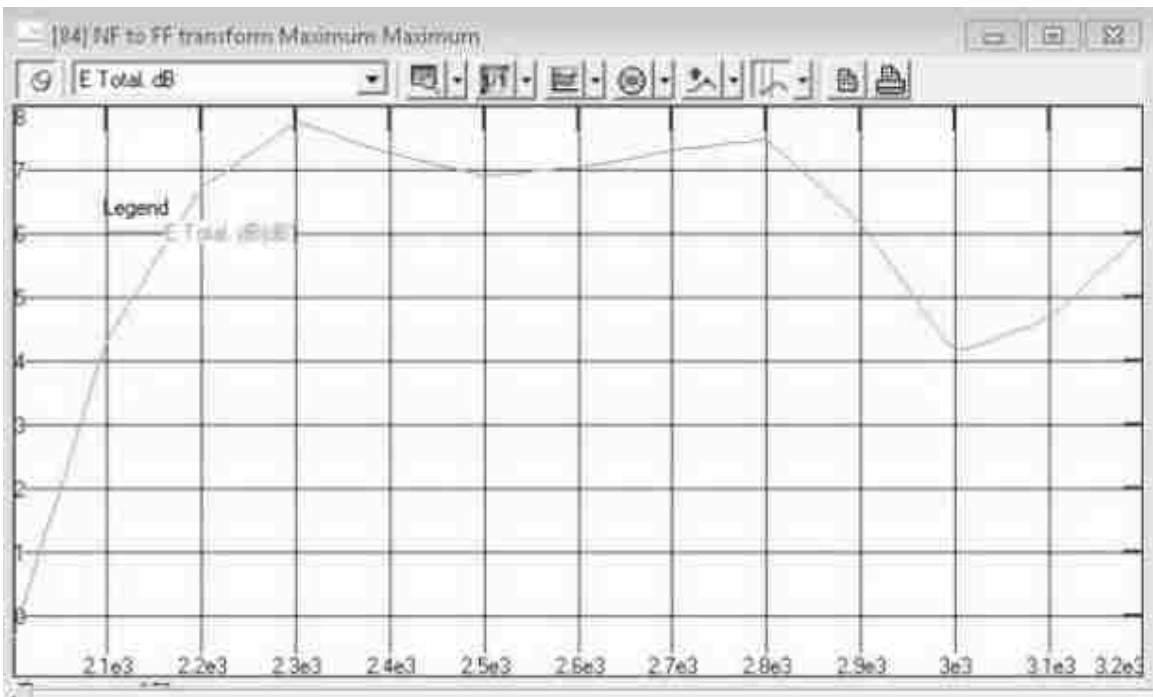


Figure 67. Measured Satimo Gain dB Results

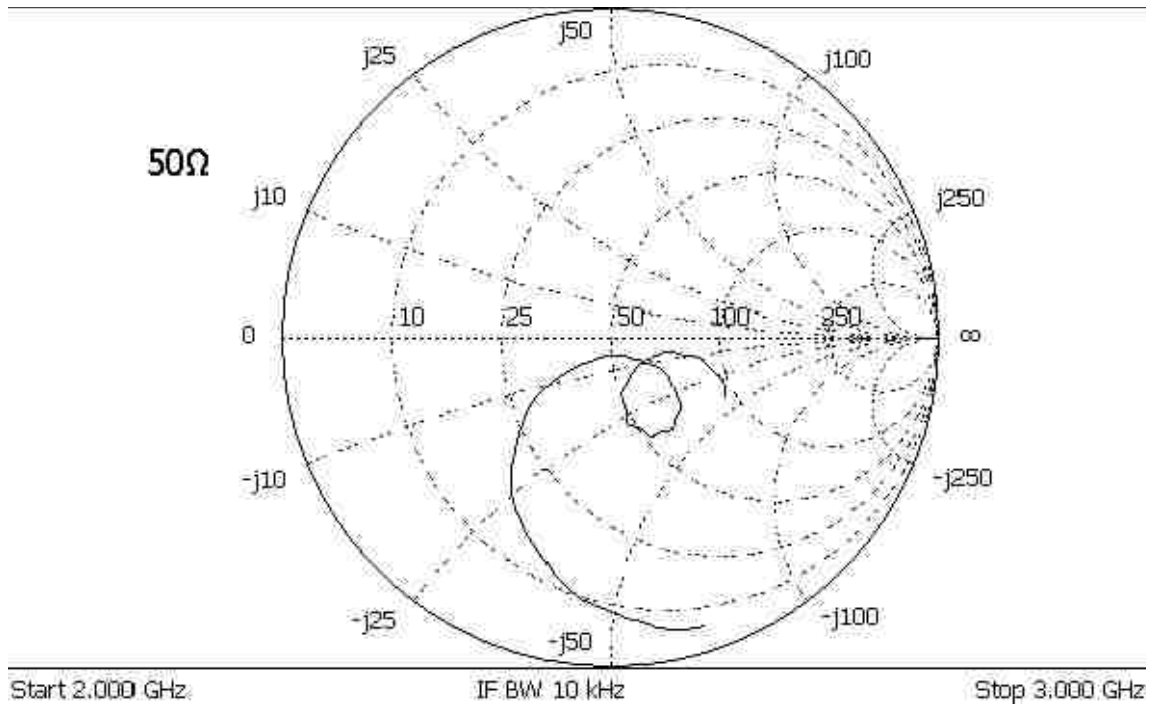


Figure 68 Measured VNA Impedance Locus

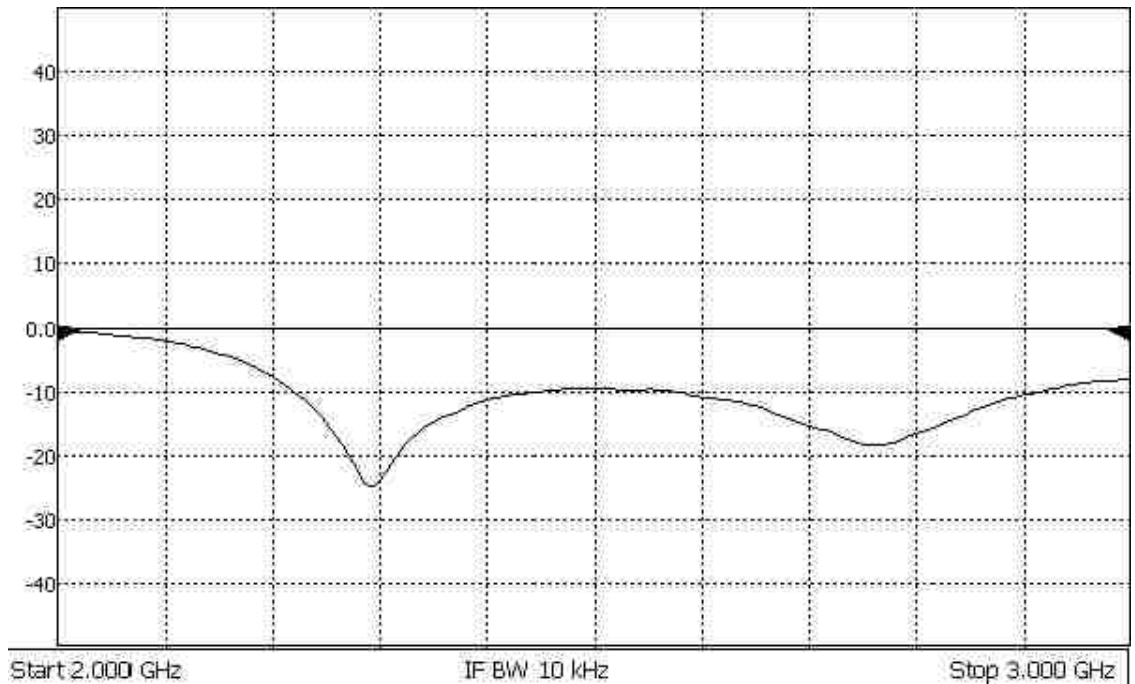


Figure 69. Measured VNA Log Magnitude

The impedance locus results in Figure 68 show the loop in the Smith chart is shifted downwards compared to the simulation results although a bandwidth of 28% was still achieved. The difference is most likely due to the non-idealities in the 2.5 GHz test assembly which could be corrected for by reducing the substrate height or changing the feed location. The result of reducing the substrate height in the test assembly is shown in Figure 70 and 71.

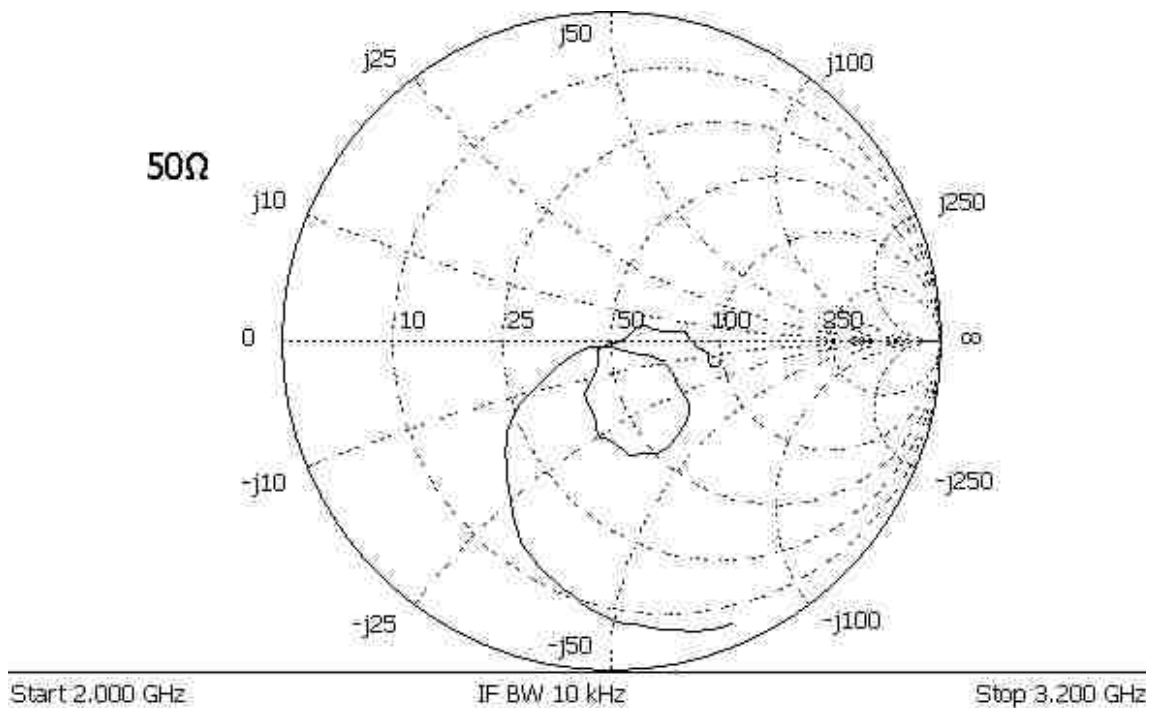
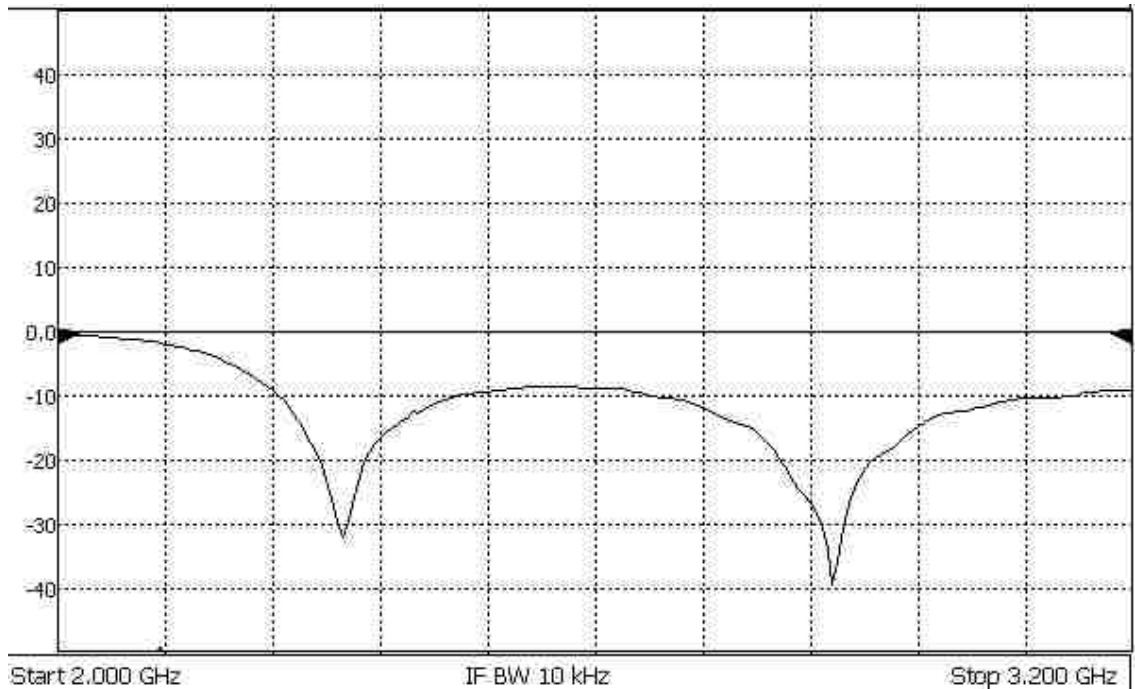


Figure 70. Measured VNA Log Magnitude with Thinner Substrate



Log Magnitude

Figure 71. Measured VNA Log Magnitude with Thinner Substrate

Figure 70 and 71 show the measured results now more closely match the simulated results however the feed location would need to be changed to keep the bandwidth under the -10dB level. The fabricated 2.5 GHz U-slot MPA test results are summarized and compared to the expected and simulated results in Table 3.

Results	Center Frequency	Bandwidth
Expected	2.5 GHz	30%
Simulated	2.53 GHz	30%
Measured	2.57 GHz	28%

Table 3. Comparison Between Various Results for the 2.5 GHz U-Slot MPA

The design proceedings and test results in this section have demonstrated an effective method for creating wideband U-slot antennas while confirming the U-slot system's wideband behavior is the result of the in-phase and out-of-phase coupling between the slot and patch resonators described by CMT.

Conclusions

By utilizing three levels of analysis and U-slot MPA circuit models, the nature of wideband behavior and related characteristics have been identified. With the CMA modal charge distributions and CMT, it was explained how the rectangular patch and U-slot resonators couple together at a lower, in-phase frequency, and a higher, out-of-phase frequency. The coupling results in the two resonant modes observed in the CMA analysis. CMT and CMA was also used to find the uncoupled resonant frequency of the rectangular patch as well as the unnormalized coupling coefficient. The uncoupled rectangular patch frequency was verified by removing the U-shape slot resulting in a resonant patch mode appearing at the center frequency. Determining the uncoupled resonant frequency of the U-slot is more complex and requires further study; though, according to CMT, is expected to be near 0.95 GHz. The U-slot MPA circuit model demonstrated how the stagger tuned input impedances of the two resonant modes results in a loop in the Smith chart and ultimately the wideband behavior of the system.

The U-slot MPA behavioral characteristics were observed through the analysis of the original U-slot MPA design and further verified by the subsequent 2.5 GHz U-slot MPA design; a process which revealed probe feed inductance may not always be ignored. If probe feed inductance is an issue, it can be corrected with the addition of series feed capacitance. It was also noted that the unstable radiation patterns result from a third, sub-resonant characteristic mode. Nulls in the S_{11} log magnitude plots were discovered to not correspond to the resonant frequencies of the patch, U-slot, or relevant characteristic modes. Contrary to widely held beliefs, the U-slot and the rectangular patch most likely resonate at or around the same frequency according to CMT.

When fabricating U-slot MPAs, it was discovered that any FR4 in-between the metallization of the patch and the substrate adversely effected the performance. Therefore, both the original and the 2.5 GHz U-slot MPAs were assembled and tested with the metallization face down on the substrate placing it in-between the FR4 and the substrate. The U-slot MPA is also very sensitive to any dielectric material within the U-shaped slot, requiring the cutting of the U-shaped slot into the FR4 backing. Ideally the U-slot MPA should be directly attached to the desired substrate which simplifies the fabrication assembly and eliminates differences between the simulation and the tested assembly. Although the test assemblies for both fabricated U-slot designs were not ideal, they demonstrated satisfactory results were achievable for very little cost while providing flexibility during testing and experimentation.

Future Work

The design method presented for creating U-slot MPAs is a general approach for achieving the proper modal behaviors and impedance locus required for wide bandwidth. Refining the approach with additional experiments on other U-slot MPA designs over a wide range of frequencies is required to characterize the approach's strengths and weaknesses as well as further support the theory.

Additional work includes characterizing the unifying principles of broadband MPA's through the analysis of other slot resonators, such as the E-slot [31], as well as analyzing other dual resonator MPA configurations such as the staked MPA [32]. It is hypothesized that a similar coupling phenomenon observed in the U-slot MPA is behind the behavior of other wideband, multi-resonator MPA configurations. Incorporating K and Q into the design process would provide additional capabilities which would help determine parameters that need to be met to maximize the bandwidth of a given U-slot MPA design. The Q of the resonant modes can be optimized for bandwidth as described in [33] while the K value can determine how far apart the two resonant modes could be from the center frequency or the uncoupled resonator frequencies and still achieve wideband performance.

Due to the complexity of the U-slot MPA, determining the uncoupled resonant frequency of the U-shaped slot is challenging. While CMT analysis does not necessarily require this value to be known, it would be helpful in the design

process for determining the ideal U-slot dimensions. This would ultimately reduce the amount of tuning required to achieve satisfactory results.

References

- [1] D. D. Grieg and H. F. Engelmann, "Microstrip-A New Transmission Technique for the Kilomegacycle Range," in *Proceedings of the IRE*, vol. 40, no. 12, pp. 1644-1650, Dec.1952.
- [2] G. A. Deschamps, "Microstrip Microwave Antennas," Third Symposium on the USAF Antenna Research and Development Program, University of Illinois, Monticello, Illinois, October 18-22, 1953
- [3] Woo, Hyoungwan and Khan, Arifur and Masui, Hirokazu and Cho, Mengu and Miyakawa, Takehiro and Fujita, Tatsuhito, "Discharge Observation on Antenna Surface Radiating High-power Microwaves in Simulated Space Environment," in TRANSACTIONS OF THE JAPAN SOCIETY FOR AERONAUTICAL AND SPACE SCIENCES, AEROSPACE TECHNOLOGY JAPAN. 12. 11-19. 10.2322/tastj.12.11. 2014.
- [4] R. E. Munson, "Conformal microstrip antennas and microstrip phased arrays," *IEEE Transactions on Antennas and Propagation*, January 1974, Vol. 22, No. 1, pp. 235-236.
- [5] R. Bancroft, *Microstrip and Printed Antenna Design*, 2nd Edition, SciTech Publishing Inc, Raleigh, NC, 2009.

[6] Y. T. Lo, D. Solomon, and W. F. Richards, "Theory and experiment on microstrip antennas," *IEEE Transactions on Antennas and Propagation*, 1979, AP-27, pp.137-149

[7] Lee, H.F., and Chen, W., eds., "Advances in Microstrip and Printed Antennas," New York: John Wiley and Sons, 1997, pp.223-242.

[8] Gan, Y.-B., Chua, C.-P., and Li, L.-W., "An enhanced cavity model for microstrip antennas," *Microwave and Optical Technology Letters*, March 2004, Vol. 40, No. 6, pp. 520-523.

[9] W. L. Stutzman and G. A. Thiele, *Antenna Theory and Design*, Third Edition, John Wiley & Sons, Inc, New York, 2013.

[10] R. J. Garbacz, *A generalized expansion for radiated and scattered fields*, Ohio State Univ., 1968.

[11] R. Harrington and J. Mautz, "Theory of characteristic modes for conducting bodies," in *IEEE Transactions on Antennas and Propagation*, vol. 19, no. 5, pp. 622-628, Sep 1971.

- [12] R. Harrington and J. Mautz, "Computation of characteristic modes for conducting bodies," in *IEEE Transactions on Antennas and Propagation*, vol. 19, no. 5, pp. 629-639, Sep 1971.
- [13] M. Cabedo, "Systematic Design of Antennas Using the Theory of Characteristic Modes," Ph. D Dissertation UPV Feb. 2007.
- [14] T. Huynh and K. F. Lee, "Single-layer single-patch wideband microstrip antenna," in *Electronics Letters*, vol. 31, no. 16, pp. 1310-1312, 3 Aug 1995.
- [15] M. Khan and D. Chatterjee, "Characteristic Mode Analysis of a Class of Empirical Design Techniques for Probe-Fed, U-Slot Microstrip Patch Antennas," in *IEEE Transactions on Antennas and Propagation*, vol. 64, no. 7, pp. 2758-2770, July 2016.
- [16] N. P. Yadav, A. Mishra, P. Singh, J. A. Ansari and B. R. Vishvakarma, "A broadband U-slot loaded circular disk patch antenna," *2009 International Conference on Emerging Trends in Electronic and Photonic Devices & Systems*, Varanasi, 2009, pp. 317-319.
- [17] K. F. Lee, S. L. Steven Yang, A. A. Kishk and K. M. Luk, "The Versatile U-Slot Patch Antenna," in *IEEE Antennas and Propagation Magazine*, vol. 52, no. 1, pp. 71-88, Feb. 2010.

- [18] K. F. Lee, K. M. Luk, K. F. Tong, S. M. Shum, T. Huynh and R. Q. Lee, "Experimental and simulation studies of the coaxially fed U-slot rectangular patch antenna," in *IEE Proceedings - Microwaves, Antennas and Propagation*, vol. 144, no. 5, pp. 354-358, Oct 1997.
- [19] K. F. Lee, K. M. Luk, K. M. Mak and S. L. S. Yang, "On the Use of U-Slots in the Design of Dual-and Triple-Band Patch Antennas," in *IEEE Antennas and Propagation Magazine*, vol. 53, no. 3, pp. 60-74, June 2011.
- [20] K. F. Tong and T. P. Wong, "Circularly Polarized U-Slot Antenna," in *IEEE Transactions on Antennas and Propagation*, vol. 55, no. 8, pp. 2382-2385, Aug. 2007.
- [21] H. Wang, X. B. Huang and D. G. Fang, "A Single Layer Wideband U-Slot Microstrip Patch Antenna Array," in *IEEE Antennas and Wireless Propagation Letters*, vol. 7, pp. 9-12, 2008.
- [22] M. Khan and D. Chatterjee, "Characteristic modes for U-slot's feed placement," *2017 IEEE International Symposium on Antennas and Propagation & USNC/URSI National Radio Science Meeting*, San Diego, CA, 2017, pp. 743-744.

- [23] Y. Chen and C. F. Wang, "Characteristic-Mode-Based Improvement of Circularly Polarized U-Slot and E-Shaped Patch Antennas," in *IEEE Antennas and Wireless Propagation Letters*, vol. 11, pp. 1474-1477, 2012.
- [24] P. S. Hall, "Probe compensation in thick microstrip patches," in *Electronics Letters*, vol. 23, no. 11, pp. 606-607, May 21, 1987.
- [25] J. J. Adams and J. T. Bernhard, "Broadband Equivalent Circuit Models for Antenna Impedances and Fields Using Characteristic Modes," in *IEEE Transactions on Antennas and Propagation*, vol. 61, no. 8, pp. 3985-3994, Aug. 2013.
- [26] H. A. Haus, W. P. Huang. "Coupled Mode Theory. "Proceedings of the IEEE, Vol 19, No 10, October 1991.
- [27] Louisell, W. H. *Coupled mode and parametric electronics*. John Wiley and Sons Inc. New York. 1960.
- [28] K. R. Schab, J. M. Outwater, M. W. Young and J. T. Bernhard, "Eigenvalue Crossing Avoidance in Characteristic Modes," in *IEEE Transactions on Antennas and Propagation*, vol. 64, no. 7, pp. 2617-2627, July 2016.

[29] S. L. Chuang, *Physics of Optoelectronic Devices*, first edition, John Wiley & Sons, New York, 1995.

[30] H. G. Booker, "Slot aeriels and their relation to complementary wire aeriels (Babinet's principle)," in *Electrical Engineers - Part IIIA: Radiolocation, Journal of the Institution of*, vol. 93, no. 4, pp. 620-626, 1946.

[31] F. Yang, Xue-Xia Zhang, Xiaoning Ye and Y. Rahmat-Samii, "Wide-band E-shaped patch antennas for wireless communications," in *IEEE Transactions on Antennas and Propagation*, vol. 49, no. 7, pp. 1094-1100, Jul 2001.

[32] S. Long and M. Walton, "A dual-frequency stacked circular-disc antenna," in *IEEE Transactions on Antennas and Propagation*, vol. 27, no. 2, pp. 270-273, Mar 1979.

[33] Ollikainen, Jani and Vainikainen, Pertti. "Design and bandwidth optimization of dual-resonant patch antennas," Report S 252. March 2002.